

https://dspace.org/

Characterisation of manganese occurences in the Kalahari Manganese Field Constraints from highresolution 2D seismic surveys

Bibi Jogee; Musa Manzi; Nombuso Ngcobo; Moyagabo Rapetsoa; Mpofana Sihoyiya ...

https://hdl.handle.net/10539/46425
WOS

Downloaded from a DSpace repository. https://dspace.org/

Characterisation of manganese occurrences in the Kalahari Manganese Field: Constraints from high-resolution 2D seismic surveys

B.A. Jogee, M.S.D. Manzi, N.G. Maduna, M.K. Rapetsoa and M. Sihoyiya
School of Geosciences, University of the Witwatersrand, Johannesburg, Private Bag 3, WITS 2050, South Africa
e-mail: bibi.jogee1@wits.ac.za; musa.manzi@wits.ac.za; nombuso.ngcobo@wits.ac.za; moyagabo.rapetsoa@wits.ac.za; mpofana.sihoyiya@wits.ac.za

A.J.B. Smith
Palaeoproterozoic Mineralisation Research Group, Department of Geology, University of Johannesburg, South Africa
Department of Science and Innovation National Research Foundation Centre of Excellence for Integrated Mineral and Energy Resource Analysis, Department of Geology, University of Johannesburg, South Africa
e-mail: bertuss@uj.ac.za

© 2025 Geological Society of South Africa. All rights reserved.

Abstract

Manganese is an important industrial metal and has a variety of applications in the steel manufacturing, industrial and biological sectors. Most manganese deposits are sedimentary in origin and the sedimentary type comprise more than 95% of high-grade world-class manganese deposits. The Palaeoproterozoic Kalahari Manganese Field in South Africa is composed of sedimentary-hosted manganese interbedded with banded iron formation and is host to the world's largest known land-based manganese resources. High-resolution 2D reflection seismic surveys were conducted to characterise the subsurface geology of the Kalahari Manganese Field in the Severn area to delineate the manganese mineralisation and associated structures in the northern section of the Kalahari Manganese Field. The contacts between the various lithologies of the: (1) Ventersdorp and Transvaal supergroups, (2) Campbellrand and Schmidtsdrif subgroups and Koegas and Asbestos Hills subgroups, (3) Ghaap and Postmasburg groups, (4) the Makganyene and Ongeluk formations, (5) Ongeluk and Hotazel formations, (6) Hotazel and Mooidraai formations, (7) Transvaal and Keis supergroups (the pre-Gamagara unconformity), (8) Keis and Karoo supergroups, and (9) Karoo Supergroup and Kalahari Group has been imaged. The results indicate that the manganese mineralisation occurs at a depth of ~1.5 km, with the thickness of the Hotazel Formation on the seismic profiles being approximately 150 m. Several structures are observed on the seismic sections and strike north-south, northeast-southwest and northwest-southeast. The north-south striking structures are interpreted as dolerite dykes as they exhibit high seismic amplitude attenuation. Determining the location of dykes beneath the surface is important for exploration drilling and production in mining. The northeast-southwest and northwest-southeast striking structures are interpreted as reactivated normal faults and shallow dipping listric thrust faults that "stacked" or "duplicated" the lithologies. The reactivated normal faults served as pathways for mineral-rich fluid migration. The northeast-southwest and northwest-southeast striking structures are significant as these structures are associated with structurally-controlled manganese mineralisation. The pre-Gamagara and Kalahari unconformities also have supergene ore enrichment events associated with them. Reflection seismics is effective in mapping the subsurface geology and structures within the Kalahari Manganese Field.

Downloaded from http://pubs.geoscienceworld.org/gssa/sajg/article-pdf/128/1/53/7237934/53_0003_jogee_et_al.pdf?casa_token=YSLKsPTCYswAAAAA:_v2NFIsneibQLQBcqZKIsf2DmEiRjMF4t6wGBtd96Jv4JPsio5HLMrbL
by University of the Witwatersrand user

Introduction

Manganese (Mn), an industrial metal discovered in 1774, allowed the transition of humankind into the modern steel age, thus is crucial for industrial development (Gutzmer and Beukes, 1996a). The industrial metal has a variety of applications, ranging from steel manufacturing and industrial, to biological applications (Mudau, 2020). More specifically, Mn has deoxidising and desulfurising properties, thus its major application in the industry is its addition to steel to increase the ductility of steel, reducing steel structure brittleness (Mudau, 2020). Mn is hosted by a variety of deposits of various sizes, grades, and origins. Currently >95% of Mn deposits exploited are of sedimentary origin (Beukes et al., 2016). Manganese is the 12th most abundant element in the Earth's crust and is usually associated with iron (Fe). This is especially the case in Mn-enriched chemical sedimentary environments (e.g., Gutzmer and Beukes, 1995; Tsikos et al., 2003; Beukes et al., 2016; Mhlanga et al., 2023; Smith and Beukes, 2023; Smith et al., 2023). Economically viable deposits of both Mn and Fe comprise sedimentary deposits such as Proterozoic Banded Iron Formation (BIF)-hosted Manganese Formations (MnFs), black shale-hosted carbonate deposits, Neoproterozoic glacially associated BIF-hosted deposits and shallow marine oolitic deposits (Beukes et al., 2016). The metallogenesis of the deposits is controlled by physicochemical properties that are inherent in Mn and Fe (e.g., Beukes et al., 2016; Mhlanga et al., 2023; Smith and Beukes, 2023). These deposits are not evenly distributed through Earth's history as formation of these deposits depends on complex interactions between the ocean-atmosphere-lithosphere-biosphere system and show distinct peaks of deposition at certain times in Earth's history. A prominent example of such deposits are the BIFs that peak in the Late Archaean and Early Palaeoproterozoic (e.g., Klein, 2005; Beukes and Gutzmer, 2008) and host the world's largest Fe ore deposits (e.g., Smith and Beukes, 2016; Angerer et al., 2022). These are closely followed by Mn formations formed in the Palaeoproterozoic close to and during the Great Oxidation Event (GOE) (Schröder et al., 2011; Beukes et al., 2016; Gumsley et al., 2017; Mhlanga et al., 2023). Proterozoic BIF-hosted Mn-rich chemical sedimentary rocks, termed Manganese formation (MnF), is the most important source of Mn (Beukes et al., 2016). This deposit type is found in the Palaeoproterozoic Kalahari Manganese Field (KMF) of South Africa which hosts the world's largest known Mn resource.

In the Griqualand West region, significant Mn and Fe ore deposits are present (Beukes and Gutzmer, 1996a; 1996b; Eriksson et al., 2006; Beukes et al., 2016; Smith and Beukes, 2016). Most of the protoliths to the Mn and Fe deposits in the Griqualand West region formed in the Palaeoproterozoic due to a variety of palaeoenvironmentally complex sedimentary processes unique to this time period, making the Mn deposits in the KMF significant in terms of understanding formation processes in Earth's history and mineral exploration. The exception to the BIF-hosted ores here is the Neoarchaean Campbellrand Subgroup carbonates, which host the ores of the Postmasburg Manganese Field (PMF) in karst structures in the central Maremane dome region (Gutzmer and Beukes, 1996b; Beukes et al., 2016). The KMF accounts for ~70% of the global Mn resource (Beukes et al., 2016; Schnebele, 2023), equating to about five billion tonnes of ore (Cairncross and Beukes, 2013). The bulk of this resource occurs as lower grade Mamatwan-type ore (~30 to 40 wt% Mn), comprising the unaltered, diagenetic MnFs of the Hotazel Formation in the Griqualand West region of the Transvaal Supergroup (Nel et al., 1986; Beukes et al., 2016). Subordinate amounts of higher grade hydrothermally enriched Wessels type ore (~42 to 60 wt% Mn) and supergene enriched ore (~40 to 42 wt% Mn) also occur (Gutzmer and Beukes, 1995; Beukes et al., 2016; Mudau, 2020). The KMF comprises six known deposits of Mn with only one deposit currently of economic importance, the Main Kalahari Deposit (MKD), while the Hotazel and Langdon deposits have been previously mined out (Caincross et al., 1997). There are three known deposits located to the north of the MKD which have been explored but not yet exploited, namely the Avontuur (Beukes et al., 2016; Coetzee et al., 2024), Leinster (Richards, 2021), and Eersbegint (Poli, 2011) deposits. From these three deposits, the Avontuur Deposit is known to contain a measured, indicated, and inferred Mn ore resource of 141.7 Mt at 38.4% Mn (Coetzee et al., 2024). The prospective Severn area in this study is located between the Leinster and Avontuur deposits and hosts Mn occurrences from both and therefore is worth exploring. The MnFs that make up the Mn ores occur as three stratiform units of variable thickness and are intercalated with four BIF units, together termed the Hotazel Formation (Beukes and Gutzmer, 1995; Tsikos et al., 2003).

Several high-resolution 2D reflection seismic surveys have been conducted to image and characterise Fe oxide deposits and proved to be successful (e.g. Malehmir and Bellefleur, 2010; Maries et al., 2017; Markovic et al., 2019; Westgate et al., 2020). Seismic surveys rely on the ability to detect contrasts in seismic velocity and density in rock units below surface, which can indicate or correlate with the presence of mineralised zones. Iron deposits exhibit higher bulk densities and seismic velocities relative to regional rocks, making reflection seismics a suitable tool for detecting such deposits due to sufficient impedance contrast. In mineral exploration, reflection seismics is an invaluable method for characterizing the subsurface geology and structure of ore-hosting rocks. In the KMF, the BIFs have higher bulk densities and seismic velocities relative to the Mn ore layers thus, this makes reflection seismics an effective exploration tool for Mn exploration in the KMF. Exploration for Mn deposits, especially in the KMF, is essential for the industrial sector globally. Subsurface exploration drilling has confirmed the presence of Mn ores of the KMF directly to the north and south of the Severn area which, itself, has not yet been subjected to subsurface exploration drilling. The aims of this work are to characterise the subsurface geology of the KMF in the Severn area, a relatively unexplored area of the KMF, and to delineate the Mn occurrences and associated structures using high-resolution 2D reflection seismics.

Downloaded from http://pubs.geoscienceworld.org/gssa/sajg/article-pdf/128/1/53/7237934/53_0003_jogee_et_al.pdf?casa_token=YSLKsPTCYswAAAAA:_v2NFIsneibQLQBcqZKIsf2DmEiRjMF4t6wGBtd96Jv4JPsio5HLMrbL
by University of the Witwatersrand user

Regional geology

The KMF is stratigraphically located within the Hotazel Formation of the Neoarchaean to Palaeoproterozoic Transvaal Supergroup in the Griqualand West region, which borders the western section of the Kaapvaal Craton (Figure 1). On a regional stratigraphic scale, the western section of the Kaapvaal Craton consists of a granitic basement that is unconformably overlain by the Neoarchaean volcanic and sedimentary rocks of the Ventersdorp Supergroup (Westgate et al., 2020). These are subsequently overlain by the Neoarchaean to Palaeoproterozoic clastics, carbonates, Fe formations and basalts of the Transvaal Supergroup. Unconformably overlying the Transvaal Supergroup are the Meso- to Neoproterozoic sedimentary and volcanic rocks of the Keis Supergroup which are, in turn, unconformably overlain by the Phanerozoic sediments of the Karoo Supergroup (Van Niekerk and Beukes, 2019; Westgate et al., 2020; Coetzee et al., 2024). The Karoo Supergroup is overlain by the Cenozoic sediments and calcretes of the Kalahari Group (Westgate et al., 2020; Coetzee et al., 2024). The Transvaal Supergroup in the Griqualand West region is subdivided into the lower Ghaap and upper Postmasburg groups (Eriksson et al., 2006). The Ghaap

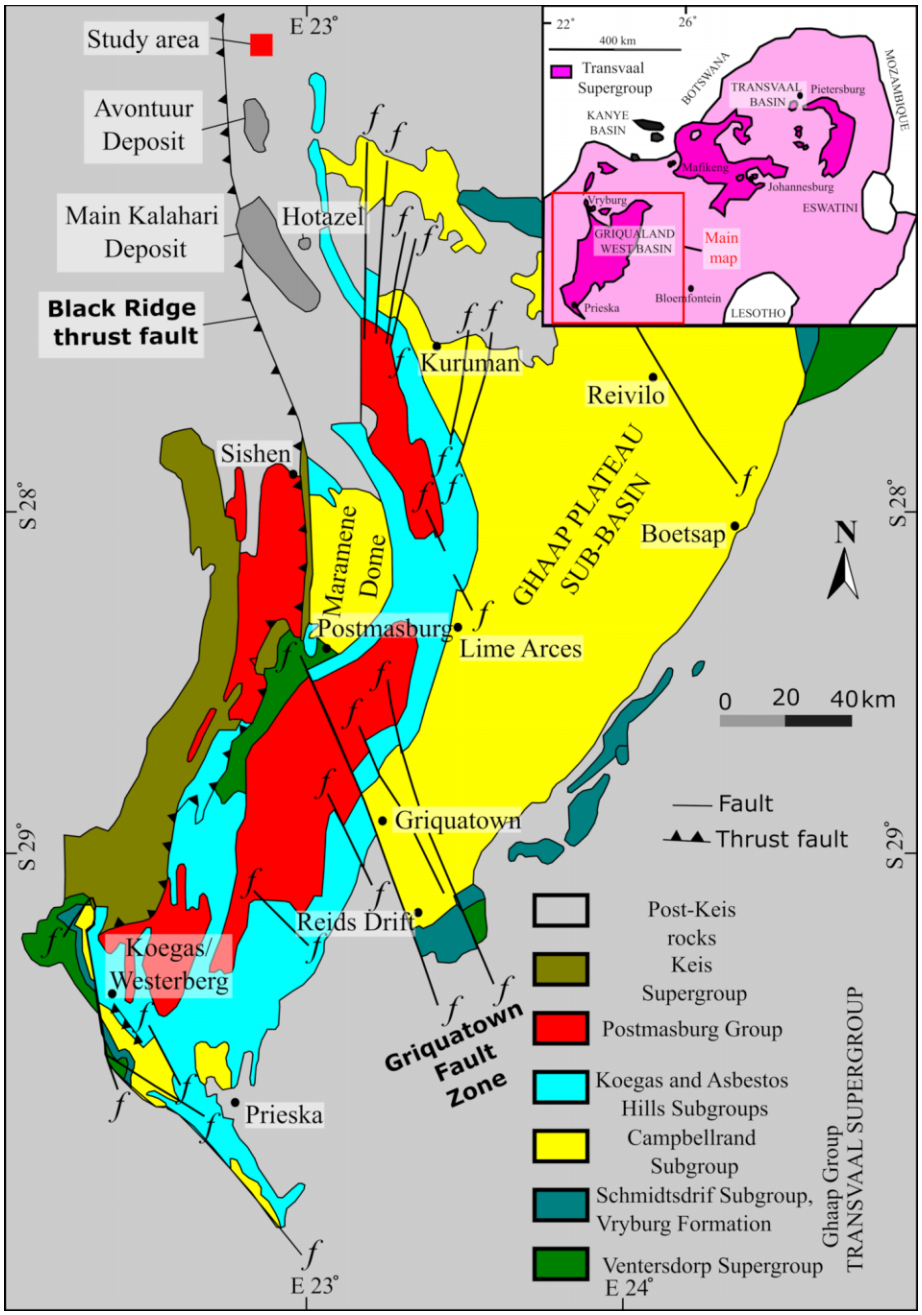


Figure 1. *Geological Map of the Griqualand-West Basin of the Transvaal Supergroup (modified after Eriksson et al., 2006). The inset shows the location of the Griqualand-West Basin within the larger Transvaal Supergroup of southern Africa.*

Downloaded from http://pubs.geoscienceworld.org/gssa/sajg/article-pdf/128/1/53/7237934/53_0003_jogee_et_al.pdf?casa_token=YSLKsPTCYswAAAAA:_v2NFIsneibQLQBcqZKIsf2DmEiRjMF4t6wGBtd96Jv4JPsio5HLMrbL
by University of the Witwatersrand user

Group is equivalent to the Chuniespoort Group of the Transvaal Supergroup in the Transvaal region, whereas correlation between the Postmasburg and Pretoria groups (the latter in the Transvaal region) is less certain due to geochronological discrepancies and unconformities (Gumsley et al., 2017). The KMF is bordered by the Kheis Metamorphic Belt to the west and the Namaqua-Natal Metamorphic Belt to the southwest (Vafeas, 2016). Deformation and metamorphism in the Kheis Belt occurred between 1 280 and 1 180 Ma and in the Namaqua-Natal Belt at approximately 1 035 Ma (Van Niekerk, 2006; Van Niekerk and Beukes, 2019). The deformation during the Kheis event was related to the formation of low angle thrusting onto the Kaapvaal Craton (Van Niekerk, 2006). One of these thrust faults is represented by the Black Ridge thrust fault (BRTF) (Beukes and Smit, 1987), which is located west of the KMF, and strikes north-south, dipping west with a 35 km displacement (Van Niekerk, 2006).

The Transvaal Supergroup in the Griqualand West region is a several kilometer-thick succession composed of carbonates, Fe formations, clastic sedimentary rocks, glacial deposits and volcanic rocks (Figures 1 to 3; Tsikos et al., 2003; Eriksson et al., 2006). The stratigraphically older Ghaap Group consists of several subgroups: the Schmidtsdrif, Campbellrand, Asbestos Hills, and Koegas subgroups (Figure 2; Beukes et al., 1986). The Schmidtsdrif Subgroup is composed of carbonates, shales, tuffites, and BIF-like cherts (Eriksson et al., 2006). The Campbellrand Subgroup comprises stromatolitic dolostone and limestone with chert interbeds and minor shale and BIF (Beukes, 1987; Altermann and Schopf, 1995; Eriksson et al., 2006; Czaja et al., 2016). The Asbestos Hills Subgroup is composed of BIF, granular Fe formation and occasional shale interbeds (Beukes, 1980; Eriksson et al., 2006; Beukes and Gutzmer, 2008). The Koegas Subgroup is composed of shales, siltstones and sandstones with minor stromatilitic carbonates and thin jaspillitic Fe formations (Eriksson et al., 2006; Schröder et al., 2011). The Ghaap Group is overlain by the Postmasburg Group within which several formations exist: the Makganyene, Ongeluk, Hotazel and Mooidraai formations (Figure 2; Beukes et al., 1986; Coetzee et al., 2024). The Makganyene Formation is composed of glacial diamictites with interbedded BIF (Le Heron et al., 2022), which are unconformably overlain by the tholeiitic basaltic-andesitic lavas of the Ongeluk Formation (Gumsley et al., 2017). The volcanic rocks of the Ongeluk Formation are conformably overlain by the interbedded BIFs and MnFs of the Hotazel Formation (Gutzmer and Beukes, 1995; Eriksson et al., 2006; Beukes et al., 2016). The Mn occurs in three MnF beds interbedded with four BIF beds (Gutzmer and Beukes, 1995; Tsikos et al., 2003). The Mooidraai Formation conformably overlies the Hotazel Formation and is composed of clastic-textured and stromatolitic carbonates with minor BIF (Bau et al., 1999; Tsikos et al., 2001; Eriksson et al., 2006; Kunzmann et al., 2014). The Hotazel and Mooidraai formations are the uppermost preserved units of the Transvaal Supergroup in the Griqualand West region and together belong to the Voëlwater Subgroup. Age constraints for the Hotazel Formation are provided by an age of 2 426 ± 3 Ma for the underlying Ongeluk Formation (Gumsley et al., 2017) and 2 394 ± 26 Ma from the overlying Mooidraai Formation (Bau et al., 1999). The combined thickness of the Mn layers is between 15 and 80 m and the whole Hotazel Formation has a combined thickness of 100 to 120 m (Gutzmer and Beukes, 1996a; Tsikos et al., 2003; Coetzee et al., 2024).

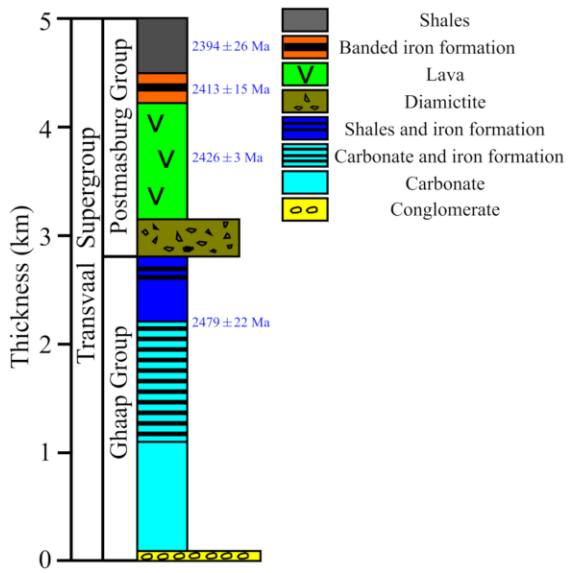


Figure 2. *Generalised lithostratigraphy for the Transvaal Supergroup in the Griqualand-West region. The ages for the Ghaap and Postmasburg groups are from Gutzmer and Beukes, 1998, Bau et al., 1999, Kendall et al., 2013 and Gutzmer and Beukes, 2017.*

The Hotazel Formation is of interest in this study as the Mn deposits are hosted within this formation. The stratigraphic setting of the Hotazel Formation suggests a shallow marine, sedimentary depositional environment in a back-arc tectonic setting (Gutzmer and Beukes, 1996a; Beukes et al., 2016). The Hotazel Formation consists of three chemo-sedimentary cycles of BIF grading upwards into hematite lutite and then Mn-rich lutite (here referred to as MnF), then back into hematite lutite and then BIF (Beukes et al., 1982; Gutzmer and Beukes, 1995; Tsikos and Moore, 1997; Coetzee et al., 2024). The three MnFs are generally referred to, from the base upwards, as the lower, middle and upper Mn beds. Most of the ore mined in the KMF comprises the unaltered hematite lutite, with approximately 3% of the MKD Mn resources occurring in higher grade ore in the northern MKD (Wessels area) that formed from hydrothermal overprints at approximately 1.28 to 1.18 and 1.05 to 1.02 Ga along mostly north-south trending normal faults (Gutzmer and Beukes, 1995; 1996a; Beukes and Cairncross, 2013; Beukes et al., 2016). Well-known mines occur in the Hotazel Formation, which include the Mamatwan, Black Rock and Wessels mines (Eriksson et al., 2006). Virtually all the Mn reserves and production originate from the lower Mn bed, which reaches maximum thicknesses of approximately 45 m at the Mamatwan mine and between 4 and 8 m at the Wessels mine (Coetzee et al., 2024).

Local geology

The geology of the area surrounding the farms in the Severn area consists of aeolian cover sands and dunes of the Gordonia Formation that form part of the Kalahari Group (Figure 4,

Downloaded from http://pubs.geoscienceworld.org/gssa/sajg/article-pdf/128/1/53/7237934/53_0003_jogee_et_al.pdf?casa_token=YSLKsPTCYswAAAAA:_v2NFIsneibQLQBcqZKIsf2DmEiRjMF4t6wGBtd96Jv4JPsio5HLMrbL
by University of the Witwatersrand user

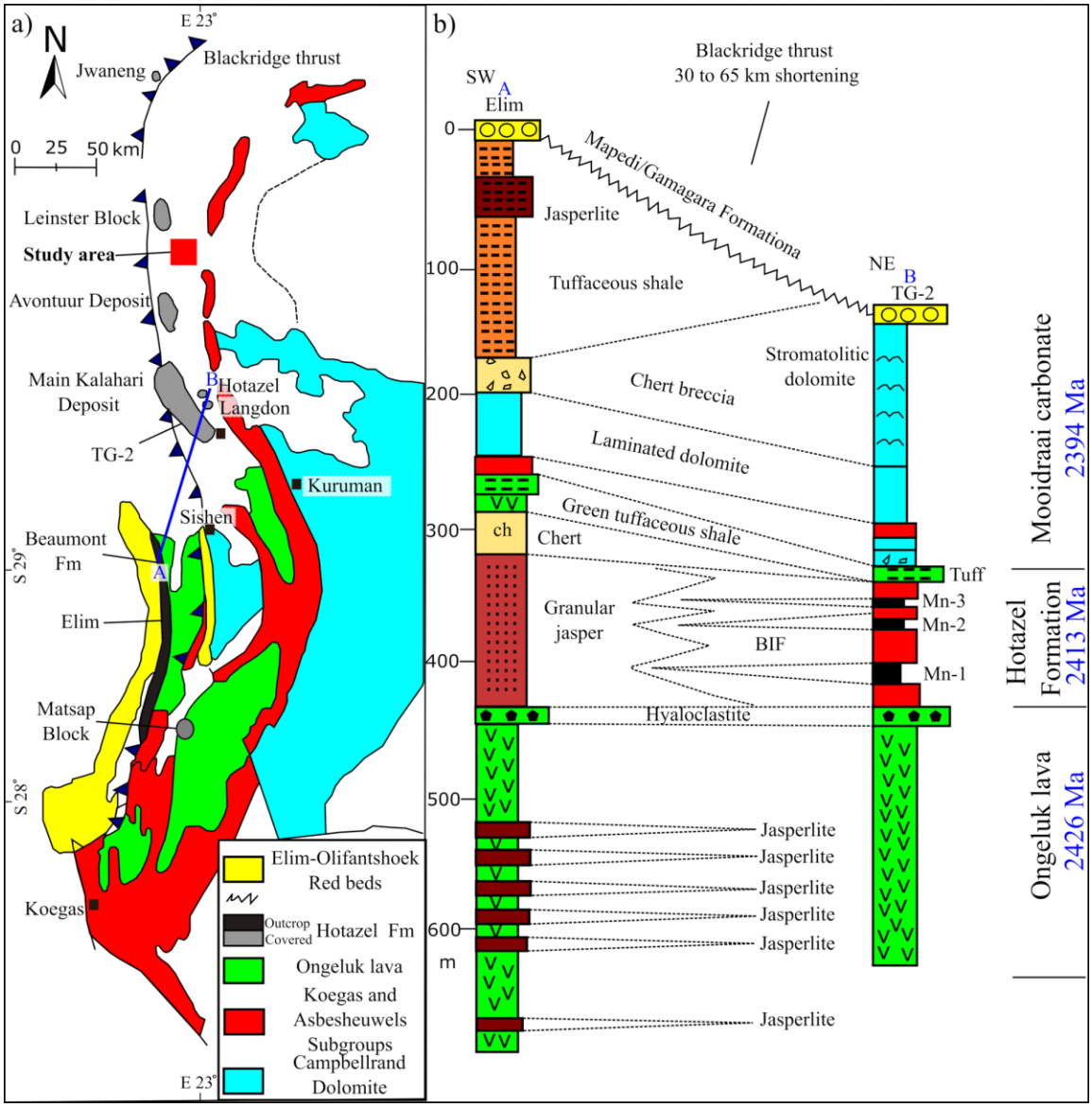


Figure 3. *(**a**) Regional map of the of the Transvaal Supergroup and lower Keis Supergroup with the study area denoted by a red star, and (**b**), lithostratigraphic sections from southwest (Sishen area) to northeast Kalahari Manganese Field (KMF) of the Ongeluk, Hotazel and Mooidraai formations (modified after Hongjun et al., 2022).*

Havenga, 2014). In the north-eastern section of the surrounding area, outcrops of basalt from the Ongeluk Formation are present (Figures 4 and 5, Havenga, 2014). The western section of the area is composed of outcrops of Fe formation of the Kuruman and Griquatown formations of the Asbestos Hills Subgroup as well as siliciclastics of the Kameelfontein Formation of the Koegas Subgroup (Figure 4, Havenga, 2014), with both subgroups forming part of the Ghaap Group. Exploration drilling has confirmed the subsurface presence of the Hotazel Formation and associated Mn mineralisation in both the Avontuur (Coetzee et al., 2024) and Leinster areas (Richards, 2021), which occur to the south and the north of Severn, respectively (Figure 4; Havenga, 2014). At both locations the Hotazel Formation is intruded by dolerite dykes. Whereas the Hotazel stratigraphy is mostly complete in the Avontuur area (Coetzee et al., 2024), it is heavily disrupted by the dolerite intrusions in the Leinster area (Richards, 2021). No subsurface drilling has been conducted in the Severn area itself, despite its proximity to the previously mentioned subsurface occurrences of the Hotazel Formation to the north and the south. No major Mn ore exploitation has yet occurred in the Avontuur and Leinster areas. The absence of subsurface drilling and prior exploitation in the Severn area makes reflection seismics a valuable and an effective method to explore for Mn deposits.

Manganese mineralisation in the Kalahari Manganese Field

As previously mentioned, three Mn ore types occur in the KMF, namely low-grade Mamatwan, high-grade Wessels, and

Downloaded from http://pubs.geoscienceworld.org/gssa/sajg/article-pdf/128/1/53/7237934/53_0003_jogee_et_al.pdf?casa_token=YSLKsPTCYswAAAAA:_v2NFIsneibQLQBcqZKIsf2DmEiRjMF4t6wGBtd96Jv4JPsio5HLMrbL
by University of the Witwatersrand user

intermediate-grade supergene ore. The primary to early diagenetic, low-grade Mamatwan-type ore (30 to 38 wt% Mn) is the most abundant ore type (~97% of MKD) and is dark brown to greyish black, microcrystalline, finely laminated and composed of finely intergrown kutnahorite, braunite, and hematite with small, but conspicuous ovoids and lenticules of Mn-bearing calcite (Gutzmer and Beukes, 1996a; Beukes et al., 2016).

The hydrothermally altered Wessels-type ore, which makes up approximately 3% of the MKD resource (Beukes et al., 2016) has been upgraded by hydrothermal fluids that infiltrated the Hotazel Formation along north-south trending normal faults to Mn grade of 46 to 55 wt% (Gutzmer and Beukes, 1995; Beukes et al., 2016). This ore type is mineralogically and texturally different from the Mamatwan-type ore. The Wessel-type ore is carbonate poor, oxide rich, and is coarser-grained. Sedimentary structures (laminations and ovoids) are obliterated by recrystallisation and therefore the ore is macroscopically relatively homogeneous in appearance and porous (Gutzmer and Beukes, 1995; Vafeas, 2016). The high-grade Wessel-type ore shows significant mineralogical and geochemical variation both vertically and horizontally. The ore has been altered to braunite II-braunite, bixbyite-hausmannite, and hausmannite-rich ore (Gutzmer and Beukes, 1995). Geochemically, the dominant ore minerals such as braunite and hausmannite contain Fe up to 22 and 15 wt%, respectively, and account for the bulk Fe content within these ores that are Fe enriched

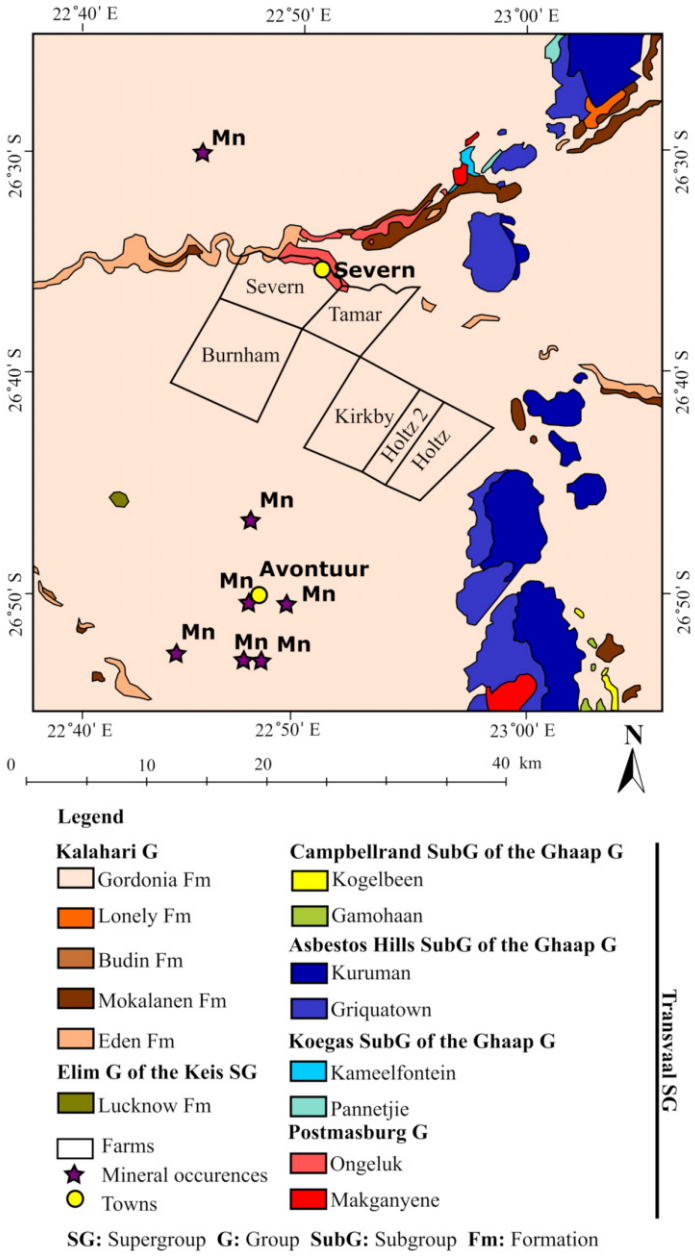


Figure 4. *Local geology of the area surrounding Severn (modified after Havenga, 2014). The area surrounding Severn mainly consists of outcrops of basalt and iron (Fe) formation. Nomenclature of stratigraphic units are based on the naming system in Botha (2021).*

Downloaded from http://pubs.geoscienceworld.org/gssa/sajg/article-pdf/128/1/53/7237934/53_0003_jogee_et_al.pdf?casa_token=YSLKsPTCYswAAAAA:_v2NFIsneibQLQBcqZKIsf2DmEiRjMF4t6wGBtd96Jv4JPsio5HLMrbL
by University of the Witwatersrand user

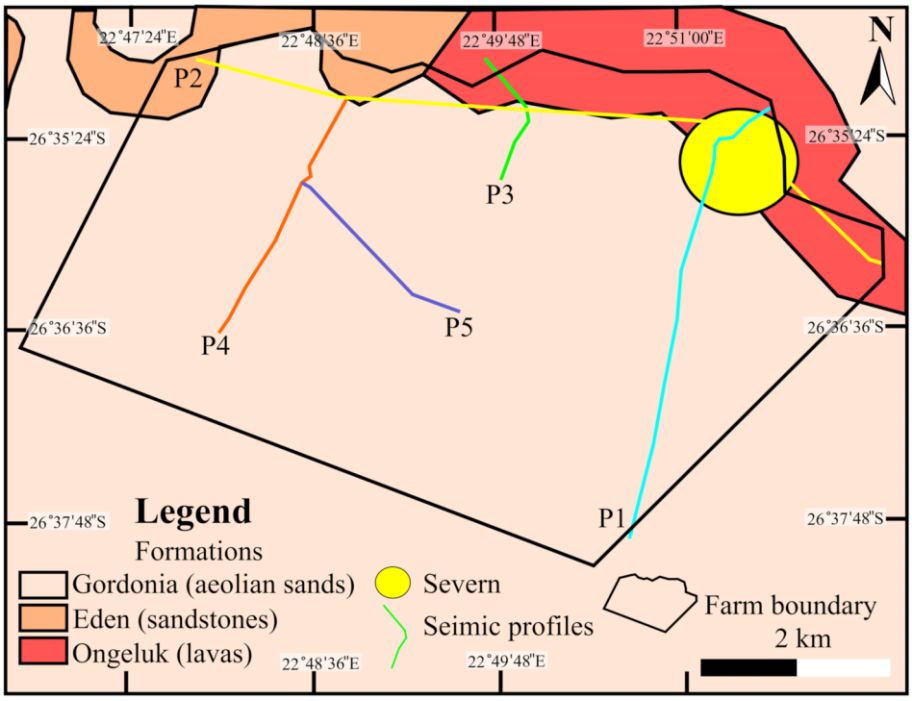


Figure 5. *Local geology map of the Severn farm, with the location of the seismic profiles across the farm boundary. The seismic profiles traverse across aeolian sands, sandstones, and lavas.*

(Mn:Fe of ~4:1) relative to Mamatwan type ores (Mn:Fe of ~8.5:1 to 10.1:1) (Beukes et al., 2016). The occurrence of Wessels-type ore is restricted to the northwestern section of the MKD where the aforementioned normal faulting as well as thrust duplication from the BRTF (Beukes and Smit, 1987) has affected the ore body (Beukes and Gutzmer, 1995; Beukes et al., 2016).

Supergene enrichment occurred twice and is present beneath the Palaeoproterozoic pre-Gamagara (also termed Mapedi) unconformity (Smith and Beukes, 2016) as well as the Cenozoic Kalahari unconformity (Gutzmer et al., 2012) and resulted from the circulation of oxygenated groundwater which percolated and leached out carbonate minerals whilst upgrading the Mn content forming supergene-type ore directly below the unconformity (Vafeas, 2018; Mudau, 2020). The interbedded BIF of the Hotazel Formation is also upgraded to high grade Fe ore where it is in direct contact with the pre-Gamagara unconformity (Smith and Beukes, 2016; Smith et al., 2019).

In the Avontuur area, which is directly to the south of the Severn area, the Mn mineralisation is dominated by the low grade Mamatwan type ore with some supergene enrichment, whereas Wessels-type high grade hydrothermal ore is mostly absent (Coetzee et al., 2024). Directly to the north of the Severn area in the Leinster area the nature of the Mn mineralisation has been hard to determine due to the disruptive nature of multiple dolerite intrusions, although lower- and higher-grade mineralisation have been documented (Richards, 2021). Due to the lack of subsurface drilling in the Severn area itself, the presence and exact nature of Mn mineralisation are unknown.

Methodology

Acquisition

In November 2023, 2D reflection seismic data were collected for the Severn project, comprising five seismic profiles with a combined total length of 18 930 m (Figure 5). These profiles were acquired within the Severn farm boundary using 1C geophones (5 Hz) (Figure 6a) connected to Remote Acquisition Units (RAUs). Receiver spacing varied, with profiles in the farm's centre at 5 m intervals and those along the main roads at 10 m intervals. The denser spacing in the centre aimed to achieve a higher resolution dataset compared to the boundaries.

Conventionally, before acquiring seismic data, we conduct tests to compare various seismic sources (i.e., 24 kg accelerated weight drop (AWD), 500 kg drop hammer, and minivibrator). However, due to logistical constraints, mobilising all the sources for testing would have been more expensive on site. Consequently, the 500 kg drop hammer (Figure 6b) was chosen for this project, primarily due to the site conditions (e.g., thick Kalahari sands). Additionally, the 500 kg drop hammer is known for its powerful impulse, making it effective for seismic profiles over 4 km and thus more cost-effective to use. Shots were recorded every 10 m across all seismic profiles, with four shot records acquired at each position and vertically stacked to enhance the signal-to-noise ratio (SNR). This process resulted in a total of 1 899 shots and 4 943 097 traces after vertical stacking.

Seismic profiles P1 and P2 were acquired along the main road, leading to some shot gathers being contaminated with noise from traffic (Figure 7a: a red shading). Seismic profile P3 was acquired along an electric fence that runs toward a water

Downloaded from http://pubs.geoscienceworld.org/gssa/sajg/article-pdf/128/1/53/7237934/53_0003_jogee_et_al.pdf?casa_token=YSLKsPTCYswAAAAA:_v2NFIsneibQLQBcqZKIsf2DmEiRjMF4t6wGBtd96Jv4JPsio5HLMrbL
by University of the Witwatersrand user

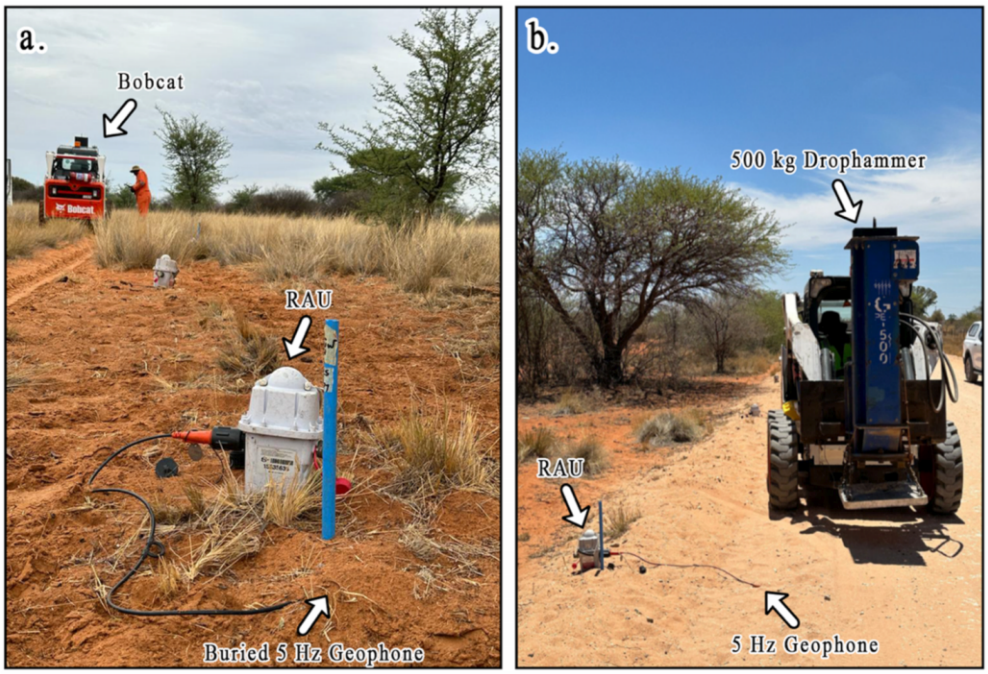


Figure 6. *(**a**) Remote acquisition unit (RAU) connected to a buried 5 Hz geophone with a 500 kg drop hammer mounted on a bobcat along the profile. (**b**) 500 kg drop hammer near a field station with RAU and a buried 5 Hz geophone for better coupling on a sandy road.*

pump. The noise characteristics of each seismic profile can be analysed by examining the frequency spectra of each profile (Figure 7k to o).

An example of a well-known noise signal in South Africa is observed in P3 (Figure 7c blue shading), where a spike at 50 Hz is caused by electric power lines (Figure 7m). Figure 7e shows high-amplitude airwaves (green shading) amplified by the soft sand cover, due to the relatively low shear wave velocity in the unconsolidated soil predominant in the project's middle sections. To mitigate this noise, careful processing techniques were applied (discussed in the next section).

Although the Remote Acquisition Units (RAUs) have built-in Global Positioning Systems, accurate receiver and shot positions (eastings, northings, and elevation) for all seismic profiles were surveyed using a real-time Differential Global Positioning System (DGPS) device, with a base station set up on stable ground. Table 1 lists the main acquisition parameters for the surface seismic survey. An event recorder was mounted on the AWD to record a GPS timestamp, which was later used to retrieve the raw shot gathers from the wireless nodes.

Table 1. Acquisition parameters for surface seismic profiles.

Survey parameters					
Profile	Mn_P1	Mn_P2	Mn_P3	Mn_P4	Mn_P5
Acquisition system	Sercel Lite	Sercel Lite	Sercel Lite	Sercel Lite	Sercel Lite
Profile length	5 890 m	5 990 m	1 580 m	3 135 m	2 335 m
Sampling rate	2 ms	2 ms	2 ms	2 ms	2 ms
Direction					
Number of receivers	590	600	317	628	468
Receiver spacing	10 m	10 m	5 m	5 m	5 m
Geophone	5 Hz	5 Hz	5 Hz	5 Hz	5 Hz
Number of shots	590	600	161	314	234
Shot spacing	10 m	10 m	10 m	10 m	10 m
Source type	500 kg Drop hammer				
Geodetic surveying	DGPS				
FFID	4 137 - 6 524	6 833 - 9 247	10 212 - 10 857	10 858 - 12 113	12 114 - 13 050

Downloaded from http://pubs.geoscienceworld.org/gssa/sajg/article-pdf/128/1/53/7237934/53_0003_jogee_et_al.pdf?casa_token=YSLKsPTCYswAAAAA:_v2NFIsneibQLQBcqZKIsf2DmEiRjMF4t6wGBtd96Jv4JPsio5HLMrbL
by University of the Witwatersrand user

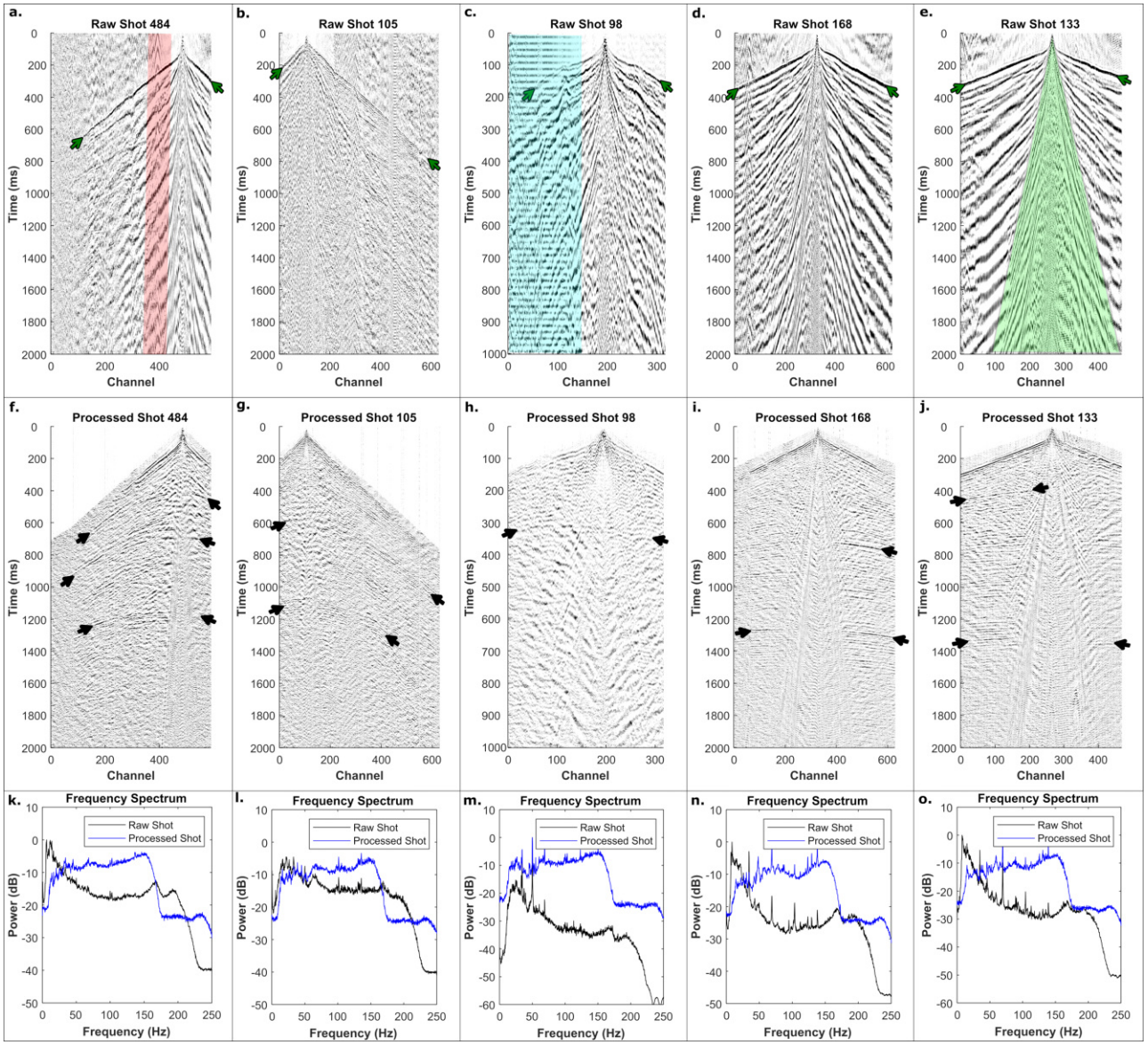


Figure 7. *Examples of raw shot gathers (**a**) to (**e**) for lines 1 to 5, respectively, showing clear first breaks (green arrows). The processed shot gathers (**f**) to (**j**) show enhanced shallow reflections (black arrows) after applying the pre-stack processing workflow. The power spectrum graph of the raw (black) and processed (blue) shot gathers are shown in (**k**) to (**o**). Traffic noise (red shading), electrical noise (blue shading), and airwaves (green shading) are highlighted.*

Data processing

The processing workflow applied to all the profiles is summarized in Table 2. The seismic data are of good quality, exhibiting clear P-wave first breaks on raw shot gathers, as indicated by the green arrows in Figure 7 (a to e). Several reflections within the shallow subsurface are observed in the processed shot gathers, marked by black arrows in Figure 7 (f to j). The processing workflow adheres to a standard procedure for reflection seismic data processing.

For both refraction statics and tomography purposes, the first break picking was initially conducted using an automatic picking algorithm. This was followed by a manual correction of any incorrect automatic picks. The calculation of refraction statics resulted in final root mean square (RMS) errors up to 5 ms, with individual profile details provided in Table 2. After the shot stacking process, the data were corrected to a fixed, final datum: 1030 m for profiles 1 and 2, 1 015 m for profile 3, and 1 025 m for profiles 4 and 5.

The data are dominated by ground roll noise, which was effectively attenuated in the shot domain using a radial trace filter. This filter utilised velocities ranging from -6 500 to 6 500 m/s and a lowpass filter with a frequency range of 8 to 18 Hz. To address linear noise on the data, a horizontal median filter with a steering velocity of 3 000 m/s was applied. Additionally, an airwave filter was used to specifically

Downloaded from http://pubs.geoscienceworld.org/gssa/sajg/article-pdf/128/1/53/7237934/53_0003_jogee_et_al.pdf?casa_token=YSLKsPTCYswAAAAA:_v2NFIsneibQLQBcqZKIsf2DmEiRjMF4t6wGBtd96Jv4JPsio5HLMrbL
by University of the Witwatersrand user

Table 2. Processing steps for the reflection seismic datasets of P1, P2, P3, P4, and P5.

Step	Process	Parameters
1	Data input	Read SEGD data, convert to HDF5
2	Stack shots	4 repeated shot records, diversity stacked
3	Geometry setup	5 m (P1-P2), and 2.5 m (P1-P5) CMP spacing, crooked line binning
4	Trace editing	Remove noisy, dead, and unbinned traces
5	First break picking	All available offsets
6	Refraction statics	P1: Datum: 1 030 m, replacement velocity: 1000 m/s P2: Datum: 1 030 m, replacement velocity: 1000 m/s P3: Datum: 1 015 m, replacement velocity: 1000 m/s P4: Datum: 1 025 m, replacement velocity: 1000 m/s P5: Datum: 1 025 m, replacement velocity: 1000 m/s
7	Radial trace filter	Vrange: -6 500 : 6 500 m/s and Lowpass filter: 8 to 18 Hz
8	Horizontal median filter	Steering velocity: 3 000 m/s
8	Airwave filter	Velocity: 350 m/s
9	Wiener deconvolution	Gap: 2 ms and length: 90 ms
10	Bandpass filter	4 – 10 – 150 – 200 Hz
11	Residual statics	Surface consistent (looped)
12	Migration	Isotropic Kirchhoff pre-stack time migration
13	NMO and stacking	Interval velocity model and Normalise (Squar Root normalisation) and Smooth stack
14	Post-stack processing (Spherical divergence, Semblance smoothing, and Spectral Weighting)	(Grid controlled velocity interpolation, Tau-P coherency filter, and 5 to 150 Hz frequencies scaled by factors from 0.25 to 3)
15	Time-to-depth conversion	Smoothed migration velocities

attenuate linear noise associated with airwaves, which travel at a velocity of 350 m/s.

To enhance reflections, eliminate multiples, and broaden the frequency spectrum, Wiener deconvolution was employed. This deconvolution process featured a gap length of 2 ms and a filter length of 90 ms. Following this, a bandpass filter was applied to retain frequencies between 10 and 150 Hz, ensuring that the signal of interest was preserved while unwanted noise was minimised.

Pre-stack processing improved the quality of the shot gathers, as illustrated in Figure 7 (f to j). To further enhance the signal-to-noise ratio of the data, multiple passes of velocity analysis were conducted both before and after surface-consistent residual statics. A detailed, semblance-based velocity analysis was performed every hundredth Common Midpoint (CMP), referencing constant velocity stacks to ensure the enhancement of genuine reflection events.

To accurately position reflections in their true subsurface locations, isotropic Kirchhoff pre-stack time migration was applied to all the profiles. Post-stack processing included several filters (e.g., deconvolution) to improve the quality of the reflections on the stacked sections before time-to-depth conversion. These techniques comprised spherical divergence correction, a Tau-P coherency filter, and spectral weighting.

The spherical divergence correction adjusted for the amplitude decay due to wavefront spreading, ensuring more consistent amplitude across the dataset. The Tau-P coherency filter was applied to enhance coherent reflections and suppress random noise, while spectral weighting balanced the frequency content, making the reflections more distinct. These post-stack enhancements significantly improved the clarity and continuity of the reflections, facilitating more accurate interpretation and analysis of the subsurface features.

Seismic interpretation

After data processing, the 2D seismic profiles were interpreted using a workflow that included the following steps:

- data preparation,
- volume-based seismic attribute analysis,
- surface mapping and surface-based seismic attribute analysis, and
- fault mapping.

Data preparation

The seismic survey was imported as SEG-Y files in the depth domain, using the UTM 35S coordinate reference system. The data exhibit a dominant frequency of approximately 100 Hz, an average P-wave velocity of 5 800 m/s, and a wavelength of 58 m. Based on the half dominant wavelength criteria, the P-wave vertical seismic resolution limit is approximately 29 m. Features smaller than this limit cannot be resolved in the dataset, although they can still be detected through seismic attribute analysis. Seismic attributes serve as filters that enhance specific

Downloaded from http://pubs.geoscienceworld.org/gssa/sajg/article-pdf/128/1/53/7237934/53_0003_jogee_et_al.pdf?casa_token=YSLKsPTCYswAAAAA:_v2NFIsneibQLQBcqZKIsf2DmEiRjMF4t6wGBtd96Jv4JPsio5HLMrbL
by University of the Witwatersrand user

geological and geophysical properties of interest within the dataset (Chopra and Marfut, 2005, 2007).

Volume-based seismic attribute analysis

Structural smoothing was applied to the original amplitude volume to enhance the resolution SNR of the seismic data (Figure 8). This attribute was particularly useful in improving the resolution of the near-surface data by enhancing the continuity of the near-surface reflections. The technique uses a Gaussian filter along with mean and median filters to smooth the input signal (Randen, 2000). The original seismic slices were conditioned using the structural smoothing volumetric attribute, with the "plain" parameter applied, and orientation window sizes set to 1.5 for the X, Y, and Z axes. Trace automatic gain control (AGC) was applied over a RMS window of nine in the seismic dataset to boost weak amplitudes particularly along the edges of the seismic sections.

Surface mapping and surface-based seismic attribute analysis

The 2D seismic lines were analyzed using the seismic-to-sequence stratigraphic method initially proposed by Mitchum et al. (1977). Bounding surfaces were selected based on high-amplitude reflectors that dominated the dataset (Figures 9, 10 and 11). The bounding surfaces were primarily picked through manual interpretation, where a freeform curve was drawn along the desired stratigraphic horizon. In some regions, auto-tracking was used, allowing automatic tracking of horizons across the seismic section. The picked horizons were converted into geological surfaces using the convergent interpolation gridding algorithm for all surfaces. The geometry of the output surfaces was automatically derived from the horizon interpretation, with grid cell sizes in both the X and Y directions set at 50 increments. Surface-based attributes, including dip angle and dip azimuth, were applied to each surface once sufficient interpretation was completed (Figure 10). These surface attributes are highly effective in fault mapping, as they provide detailed information on the stratigraphic and structural elements of the region (Cox et al., 2020).

Fault mapping

The primary indicators for detecting faults in a seismic section include the vertical displacement of an otherwise continuous reflector (i.e., stratigraphic surface) and the abrupt termination of a seismic event. Fault identification was conducted through manual interpretation, similar to manual horizon picking, where specific points between the hanging wall and footwall blocks of a fault boundary were delineated. Fault interpretations were marked as vertical lines in the seismic sections (Figure 12).

Results and interpretation

Seismic observations

The seismic profiles traverse across aeolian sands, sandstones and volcanic rocks (Figure 5). From the processed profile lines 1, 2, 3, 4 and 5, nine distinct, nearly horizontal, high amplitude reflections are observed at various depth intervals: 0.05, 0.30, 0.70, 1.05, 1.35, 1.70, 2.24, 2.81, and 3.42 km (Figures 9, 10 and 11). These high-amplitude reflections correspond to the contacts between the various lithologies within the Kalahari Group, Karoo Supergroup, Keis Supergroup, Transvaal Supergroup,

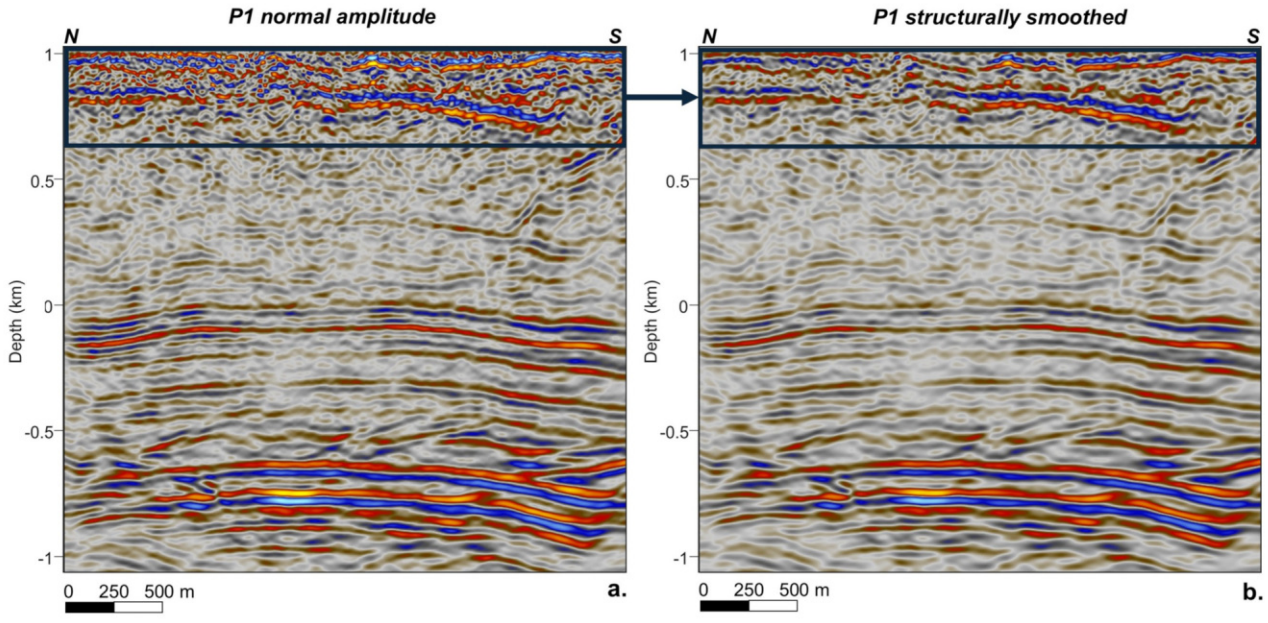


Figure 8. *2D interpretation window of the processed seismic profile (P1) comparing (**a**) the original seismic data and (**b**) the structural smoothing attribute. The near-surface resolution in (b) has been significantly improved compared to the original seismic profile (a).*

Downloaded from http://pubs.geoscienceworld.org/gssa/sajg/article-pdf/128/1/53/7237934/53_0003_jogee_et_al.pdf?casa_token=YSLKsPTCYswAAAAA:_v2NFIsneibQLQBcqZKIsf2DmEiRjMF4t6wGBtd96Jv4JPsio5HLMrbL
by University of the Witwatersrand user

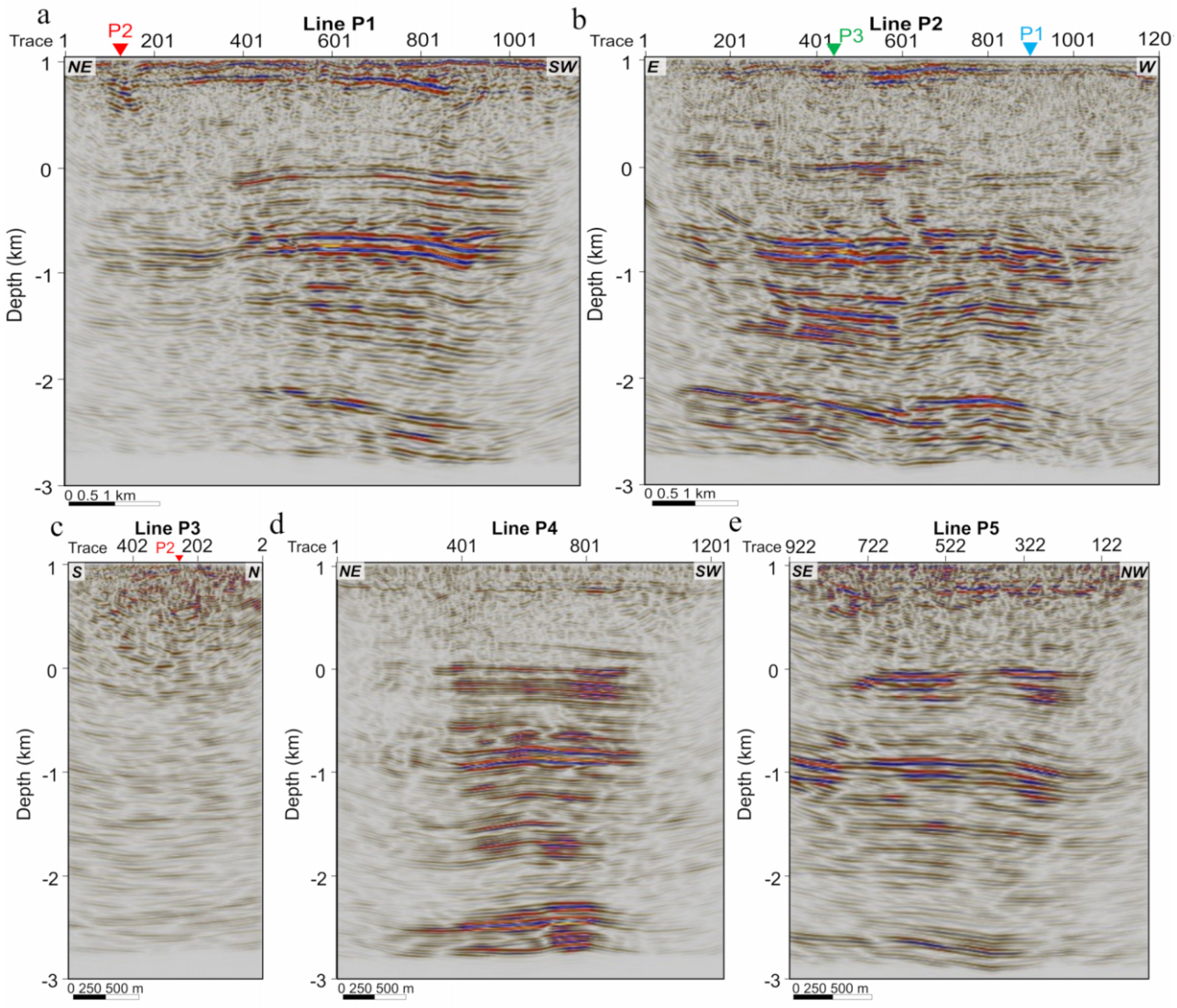


Figure 9. *All the acquired and processed seismic profiles (**a**) P1, (**b**) P2, (**c**) P3, (**d**) P4 and (**e**) P5. High amplitude reflections correspond to lithology contacts in the Kalahari Group, Karoo Supergroup, Keis Supergroup, Transvaal Supergroup, and Ventersdorp Supergroup.*

and Ventersdorp Supergroup. The nine high-amplitude horizons are numbered in Figure 10 and the various numbers, i.e., 1 to 9, from bottom to top, correspond to the contact between the (1) Ventersdorp and Transvaal supergroups, (2) Campbellrand and Schmidtsdrif subgroups, and Asbestos Hills and Koegas subgroups, (3) Ghaap and Postmasburg groups, (4) the Makganyene and Ongeluk formations, (5) the Ongeluk and Hotazel formations, (6) the Hotazel and Mooidraai formations, (7) Transvaal and Keis supergroups (the pre-Gamagara unconformity), (8) Keis and Karoo supergroups, and (9) Karoo Supergroup and Kalahari Group (Figure 11 and 12). The high-amplitude reflections between 1.05 and 1.35 km represent the BIFs of the Hotazel Formation and is the interest of this study as the mineralisation is most likely hosted within this zone. According to Westgate et al. (2020), the Kuruman Formation, a unit composed of iron-oxide mineralisation, was mapped at a depth of ~1 km. The Kuruman Formation occurs in the Asbestos Hills Subgroup of the Ghaap group which is located below the Hotazel Formation. The legacy seismic section in Westgate et al. (2020) is located north of our study area and, according to Vafeas (2016), the stratigraphic units increase in thickness from northeast-southwest, therefore, the Hotazel Formation likely occurs at a depth of ~1 km in the Severn area. The reflections between 1.05 and 1.35 km depth are moderate and represents the contact between the Mooidraai and Hotazel formations. The reflections are moderate as the Mooidraai Formation, which overlies the Hotazel Formation, is composed of clastic-textured and stromatolitic carbonates with minor BIF. Thus, the moderate reflections are due to relatively similar velocities of the dolomites of the Mooidraai Formation and BIFs of the Hotazel Formation. A similar scenario is documented by Westgate et al. (2020) where the contact between the upper dolomites of the Schmidtsdrif Subgroup and the banded iron formations of the Kuruman Formation is shown by moderate reflections.

Downloaded from http://pubs.geoscienceworld.org/gssa/sajg/article-pdf/128/1/53/7237934/53_0003_jogee_et_al.pdf?casa_token=YSLKsPTCYswAAAAA:_v2NFIsneibQLQBcqZKIsf2DmEiRjMF4t6wGBtd96Jv4JPsio5HLMrbL
by University of the Witwatersrand user

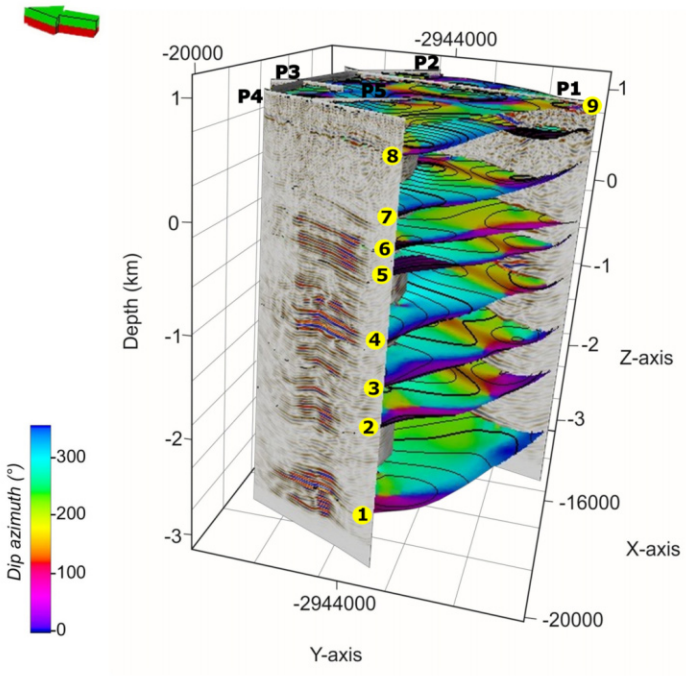


Figure 10. *3D interpretation of all the seismic profiles (P1 to P5) showing the dip azimuth of nine picked surfaces corresponding to high amplitude reflections at various depth intervals. The near-horizontal surfaces are contacts separating various lithologies from the Ventersdorp Supergroup, Transvaal Supergroup, Keis Supergroup, Karoo Supergroup, and the Kalahari Group shown in Figure 13.*

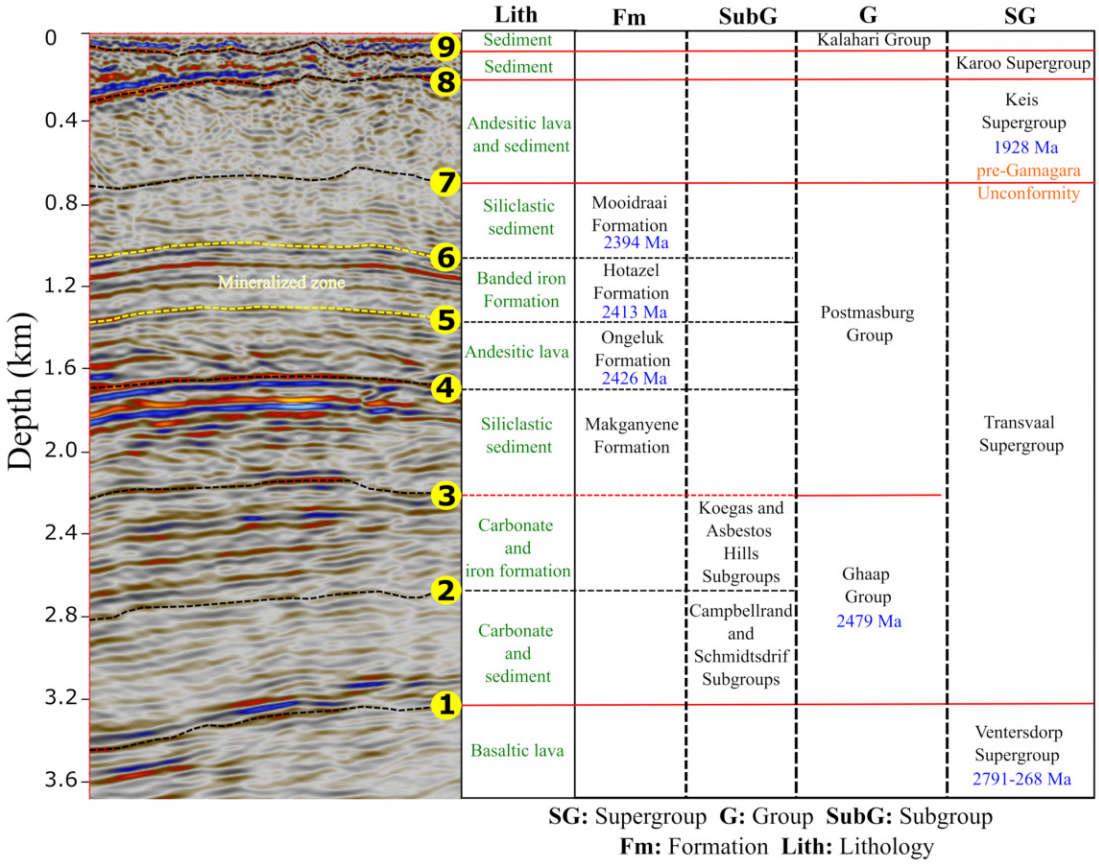


Figure 11. *2D interpretation of a seismic profile showing all the surfaces picked in the seismic dataset. The surfaces correspond to contacts separating various lithologies in the Ventersdorp Supergroup, Transvaal Supergroup, Keis Supergroup, Karoo Supergroup, and the Kalahari Group.*

Downloaded from http://pubs.geoscienceworld.org/gssa/sajg/article-pdf/128/1/53/7237934/53_0003_jogee_et_al.pdf?casa_token=YSLKsPTCYswAAAAA:_v2NFIsneibQLQBcqZKIsf2DmEiRjMF4t6wGBtd96Jv4JPsio5HLMrbL
by University of the Witwatersrand user

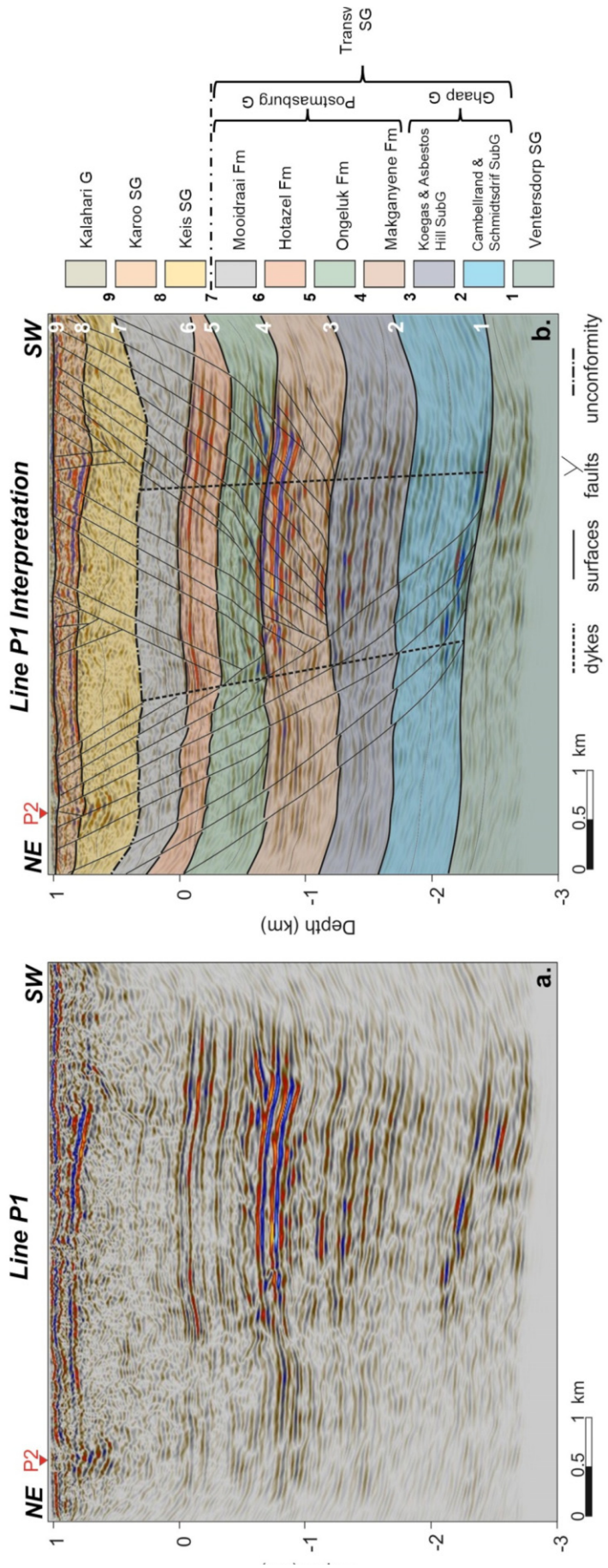


Figure 12. *Interpretation of line 1. The numbers 1 to 9, from bottom to top, correspond to the contact between the (1) Ventersdorp and Transvaal supergroups, (2) Campbellrand and Schmidtsdrif subgroups; Asbestos Hills and Koegas subgroups, (3) Ghaap and Postmasburg groups, (4) Makganyene and Ongeluk formations, (5) Ongeluk and Hotazel formations, (6) Hotazel and Mooidraai formations, (7) Transvaal and Kets supergroups (the pre-Gamagara unconformity), (8) Kets and Karoo supergroups, and (9) Karoo Supergroup and Kalahari Group. The various contacts are displaced by normal and thrust faults depicted by the solid lines (low amplitude reflection zones). The dotted lines represent the pre-Gamagara dolerite dykes.*

Downloaded from http://pubs.geoscienceworld.org/gssa/sajg/article-pdf/128/1/53/7237934/53_0003_jogee_et_al.pdf?casa_token=YSLKsPTCYswAAAAA:_v2NFIsneibQLQBcqZKIsf2DmEiRjMF4t6wGBtd96Jv4JPsio5HLMrbL
by University of the Witwatersrand user

The surfaces of the contacts between the various supergroups, groups, subgroups and formations are striking approximately north-south and have an average, near-horizontal dip angle between 0° and 5° (Figure 10 and 11). The Hotazel Formation is therefore near-horizontal in orientation (Figure 11).

Several low-amplitude reflection zones that displace the high-amplitude reflections at various depth intervals are observed in profile 1 (Figure 12). These low-amplitude reflections are striking approximately north-south, northeast-southwest, northwest-southeast, and are interpreted as faults that displaced the various lithologies and lithological contacts within the sequence (Figure 12). The interpreted faults represent relatively steeply dipping reactivated normal faults striking northeast-southwest and relatively shallowly dipping listric thrust faults striking northwest-southeast. The shallowly dipping listric thrust faults "stacked" or "duplicated" the stratigraphic sequence. The high-amplitude reflections between 1.05 and 1.35 km on profiles 1 and 2 are, therefore, displaced by the reactivated normal faults which likely served as conduits for mineralising fluids. The low-amplitude reflections striking north-south are interpreted as a north-south striking dolerite dyke.

Discussion

The Hotazel Formation and pre-Gamagara unconformity

As previously presented, the Mn deposits in the KMF are hosted within the Hotazel Formation of the Transvaal Supergroup. The Hotazel Formation is overlain and underlain by the Mooidraai and Ongeluk formations, respectively (Figure 11; Eriksson et al., 2006). For the sake of this discussion, the three MnF beds of the Hotazel Formation, which are interbedded with four BIF beds (Gutzmer and Beukes, 1996a; Tsikos et al., 2003), will be referred to as the lower manganese bed (LMB), middle manganese bed (MMB) and the upper manganese bed (UMB). The thickness of the various BIF and MnF beds ranges between 0 and 20 m, but can be up to 45 m (Gutzmer and Beukes, 1996a; Tsikos et al., 2003; Beukes et al., 2016; Mudau 2020; Coetzee et al., 2024). From the seismic profiles, between depths intervals of 1.05 and 1.35 km, several alternating high- and low-amplitude horizons are observed (Figure 11). These alternating high- and low-amplitude horizons likely correspond to the alternating layers of BIF and MnF beds (Figure 11). Iron-rich oxides in BIF such as magnetite and hematite have higher densities and P-wave velocities compared to Mn-rich minerals in the KMF such rhodochrosite and braunite. Therefore, the higher amplitude reflections correspond to the BIF and the lower amplitude reflections correspond to the MnF beds. The thickness of the Hotazel Formation on the seismic profiles is approximately 150 m and corresponds to the known thickness of the Hotazel Formation, which attains a maximum thickness of up to approximately 180 m (Kunzmann et al., 2014). The thickness of approximately 150 m may be due to thrusting causing a duplication of strata. The MnF beds occur at a depth of ~1.5 km (Figure 11). Therefore, underground mining would be a suitable mining method in the Severn area although these depth intervals may be too deep for mining Mn (Vafeas, 2016). At a depth of 0.7 km (Figure 11), high-amplitude reflections are prevalent and correspond to the contact between the Transvaal and Keis supergroups where the pre-Gamagara unconformity exists at the contact between the two (Figure 11). The first few metres directly below the pre-Gamagara unconformity are marked by the presence of ferruginous lateritic weathering that can serve as a zone of supergene enrichment for both Fe and Mn ores in both BIF and carbonate protoliths (Gutzmer and Beukes, 1996b; Smith and Beukes, 2016; Vafeas, 2016; Smith et al., 2019; De Kock et al., 2020). The seismic profiles indicate that depth intervals between 1.05 and 1.35 km are potential targets for Mn exploration in the study.

Structures and the Wessels-type ore

The Wessels-type high-grade ore is restricted to the northwestern section of the KMF and is characterised by intense deformation such as thrust duplication and normal faulting (Gutzmer and Beukes, 1995; 1996a; Tsikos et al., 2003; Mudau 2020). The normal faults have been shown to have served as conduits for mineral-rich hydrothermal fluids which led to enrichment of the Mn ore layers (Gutzmer and Beukes, 1995; 1996a; Beukes et al., 2016). After the formation of the pre-Gamagara unconformity, the KMF was affected by north-south normal faulting resulting in the down-faulting of lithologies (Vafeas, 2016). At approximately 1.2 Ga, the deformation associated with the Kheis and Namaqua-Natal orogenies occurred (Van Niekerk and Beukes, 2019), reactivating the normal faults and forming thrust faults including the BRTF (Beukes and Smit, 1987) and several minor thrust faults (Vafeas, 2016; Madua, 2020). The BRTF is situated west of the KMF and is associated with the duplication of strata (Beukes et al., 2016). Thus, in areas where strata have been duplicated (likely to the west) deposits will potentially have two ore bodies, one above and one below the thrust, respectively. The Wessels event involved the movement of hydrothermal fluids along major reactivated north-south striking normal faults and has been dated to ~1.2 to 1 Ga (Beukes and Gutzmer, 1996a). The infiltration of these fluids upgraded the Mn ores by the dissolution of carbonates and the leaching of silica from the Mn ore layers, forming the Wessels-type ore (Gutzmer and Beukes, 1995; 1996a; Vafeas, 2016). From seismic profiles 1 and 2, low-amplitude zones with northeast-southwest and northwest-southeast strikes are observed. These low-amplitude zones are interpreted as faults. The northeast-southwest striking faults are near-vertical reactivated normal faults, and the northwest-southeast striking faults are shallowly dipping listric thrust faults. The northeast-southwest and northwest-southeast faults correspond to the thrust faults that were formed from the reactivation of normal faults at approximately 1.2 Ga. The reactivated normal faults exist throughout the stratigraphy of the Transvaal Supergroup and are observed at depths between 1.05 and 1.35 km. The reactivated normal faults crosscut the Hotazel Formation and potentially enabled hydrothermal fluids to enrich the ore close to these faults. The north-south striking low amplitude reflections are interpreted as dykes. The dykes are likely doleritic in composition (dykes in the area are known to be doleritic in composition based on petrology and geochemistry

Downloaded from http://pubs.geoscienceworld.org/gssa/sajg/article-pdf/128/1/53/7237934/53_0003_jogee_et_al.pdf?casa_token=YSLKsPTCYswAAAAA:_v2NFIsneibQLQBcqZKIsf2DmEiRjMF4t6wGBtd96Jv4JPsio5HLMrbL
by University of the Witwatersrand user

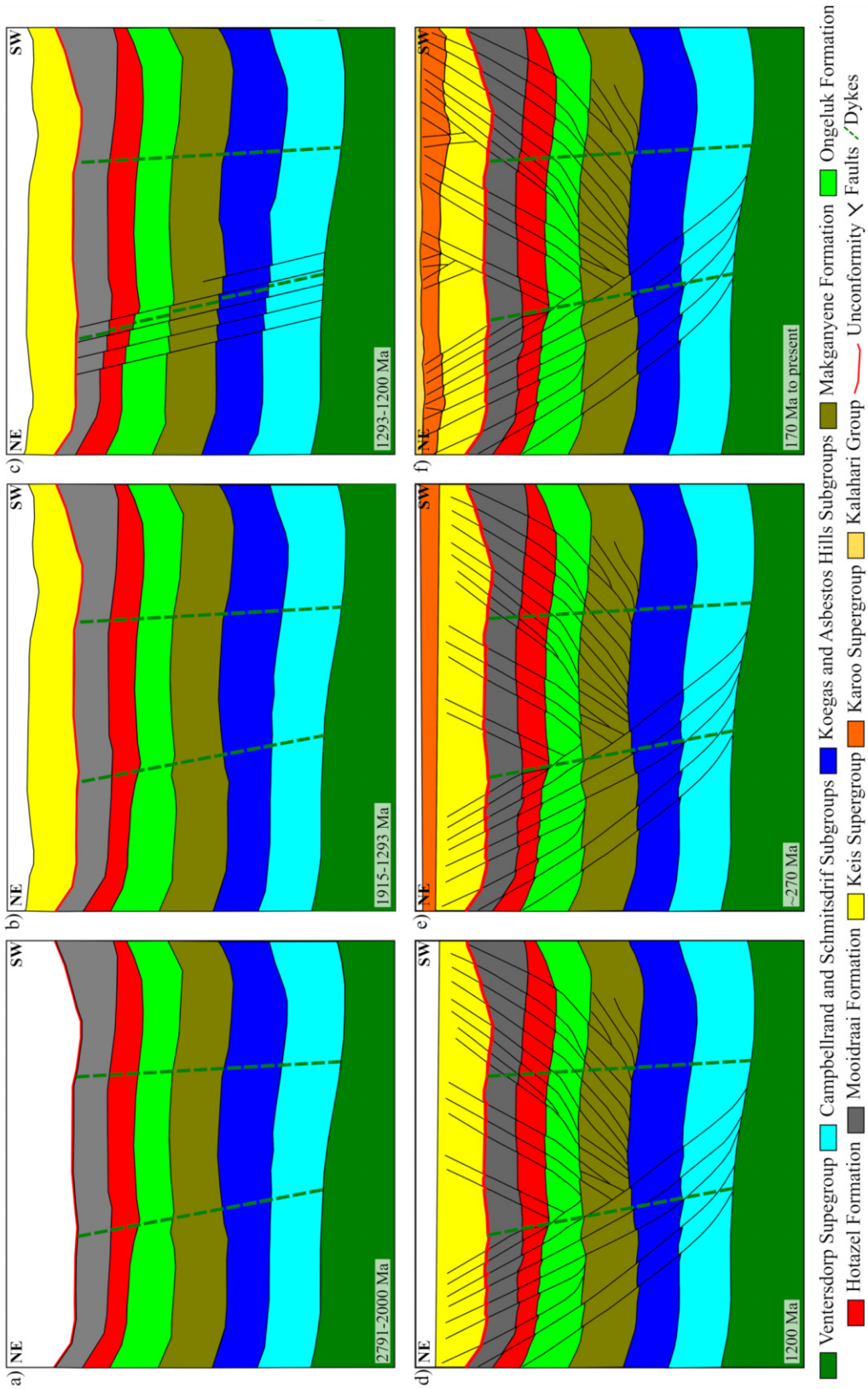


Figure 13. *Simplified tectono-metallogenetic model. (**a**) Emplacement of the andesitic lavas of the Ventersdorp Supergroup occurred followed by the deposition of the Ghaap and Postmasburg groups. The primary low-grade Mamatwan-type ore was deposited during this period. Followed by the intrusion of the pre-Gamagara aged doleritic dykes. Thereafter, a hiatus occurred associated with 200 to 400 Ma of missing geological record, during this period the pre-Gamagara erosional unconformity (red solid line) was formed at approximately 2.2 to 2 Ga. (**b**) After the formation of the pre-Gamagara unconformity deposition of the Keis Supergroup occurred. (**c**) An unknown deformation event occurred forming north-south striking normal faults which resulted in the down-faulting of the stratigraphic sequence. (**d**) Deformation attributed to the Keis Orogeny resulted in the reactivation of the normal faults forming several minor thrust faults associated with thrust duplexes. This stage involved the initiation of the early stages of the Wessels event associated with hydrothermal redistribution of manganese ore along reactivated normal faults. (**e**) Erosion occurred thereafter followed by the deposition of the Duyka Group. (**f**) The Karoo Supergroup was depositedLastly, an unknown deformation event occurred associated with neotectonics in which faults displaced both the Kalahari Group and the Karoo Supergroup.*

Downloaded from http://pubs.geoscienceworld.org/gssa/sajg/article-pdf/128/1/53/7237934/53_0003_jogee_et_al.pdf?casa_token=YSLKsPTCYswAAAAA:_v2NFIsneibQLQBcqZKIsf2DmEiRjMF4t6wGBtd96Jv4JPsio5HLMrbL
by University of the Witwatersrand user

(Vafeas, 2016)) and pre-Gamagara in age as they are crosscut by the pre-Gamagara unconformity (Vafeas, 2016). The dyke crosscuts the Hotazel Formation on the seismic profile and is known to stratigraphically disrupt the Leinster deposit making it hard to determine ore grades and continuity (Richards, 2021). Therefore, by determining the location of dykes, exploration and mining companies will be able to plan as to where to conduct exploration drilling, and ensure strategic decision making in mine plan design.

Tectono-metallogenetic model

A simplified tectono-stratigraphic model was constructed to illustrate the sequence of geological events in the region and the metallogenesis of the Mn ore layers (Figure 13). The seismic data were integrated with known geological data in the region to construct the model. The model encompasses the emplacement and deposition of various lithologies, the formation of the pre-Gamagara unconformity, and the formation of fault structures that served as pathways for mineral-rich fluids which upgraded the ore in the MnF beds of the Hotazel Formation.

The first stage of the model incorporates the extrusion of the andesitic lavas of the Ventersdorp Supergroup between 2 791 and 2 683 Ma (Figure 13a; Gumsley et al., 2020). This was followed by the formation of a sedimentary basin in which the Ghaap and Postmasburg groups of the Transvaal Supergroup were deposited after approximately 2 642 Ma (Walraven and Martini, 1995; Eriksson et al., 2006) (Figure 13a). This included the deposition of lithologies such as carbonates, iron formation, siliciclastics, glacial diamictite, basalt and MnFs. The Ghaap and Postmasburg groups are separated by an erosional unconformity formed by a glacial event that deposited the Makganyene Formation and might have been of global extent (Evans et al., 1997; Kirschvink et al., 2000; Gumsley et al., 2017; Le Heron et al., 2022). The BIFs and the interbedded MnFs of the Hotazel Formation were deposited between approximately 2 426 ± 3 Ma (Gumsley et al., 2017) and 2 394 ± 26 Ma (Bau et al., 1999). These MnFs are the diagenetic Mn-rich lutites that constitute the low grade Mamatwan type ore. Pre-Gamagara aged dolerite dykes then intruded the lithological sequence and were associated with contact metamorphism in the immediate vicinity of the contacts between the dolerite dykes and host lithologies (Figure 13a).

Thereafter, in a period marked by approximately 200 to 400 Ma of missing geological record, the Transvaal Supergroup strata were folded and then intersected by the pre-Gamagara erosional unconformity at approximately 2.2 to 2 Ga (Dalstra and Rosière, 2008; Smith and Beukes, 2016) (Figure 13b). It should be noted here that an alternative age of approximately 1 250 Ma for this or a similar unconformity east of the BRTF has been proposed (Rasmussen et al., 2020), where most of the lower Keis Supergroup (dated at ~1 915 Ma; Cornell et al., 2016) is missing due to thrusting and erosion. This proposed age also overlaps with the Kheis and Namaqua-Natal orogenies. The pre-Gamagara unconformity allowed meteoric fluids to percolate through the lithologies of the Hotazel Formation and caused supergene enrichment of the Mn ores by carbonate leaching and Mn oxidation. Consequently, a sedimentary basin formed in which the various formation of the Keis Supergroup were deposited between approximately 1 915 and 1 293 Ma (Van Niekerk and Beukes, 2019) (Figure 13b). The entire stratigraphic sequence was then affected by north-south trending normal faulting, which resulted in the down-faulting of the lithologies (Figure 13c). At approximately 1.2 Ga, deformation attributed to the Kheis and Namaqua-Natal orogenies resulted in the reactivation of the normal faults forming the BRTF and several minor thrust faults associated with thrust duplexes (Van Niekerk and Beukes, 2019) (Figure 13d). The infiltration and movement of hydrothermal fluids along reactivated north-south striking normal faults upgraded the Mn ores by the dissolution of carbonates and leaching of silica from the MnF beds. This is considered the initiation of the Wessels event, which was associated with hydrothermal redistribution of Mn and Fe along reactivated normal faults (Beukes and Gutzmer, 1995) (Figure 13d). The thrust faulting also caused duplication of the Hotazel Formation and other strata of the Transvaal and Keis supergroups, especially to the west of the KMF (Cairncross and Beukes, 2013).

No geological units are preserved between approximately 1200 and 290 Ma in the Griqualand West region, with the glacial deposits of the Dwyka Group of the Karoo Supergroup deposited in the late-Carboniferous period (Figure 13e; Bangert et al., 1999). Subsequently, at around 170 Ma, Gondwana broke up and the Karoo Supergroup lithologies were eroded to form the Kalahari unconformity, upon which the sediments of the Cenozoic Kalahari Group were deposited (Van Niekerk and Beukes, 2019) (Figure 13f). Before deposition of the Kalahari Group, another supergene enrichment event affected the Hotazel Formation MnF beds where it was in contact with the Kalahari unconformity, causing minor Mn upgrades (Gutzmer et al., 2012; Beukes et al., 2016). An unknown deformation event occurred thereafter, associated with neotectonics associated with the development of northwest-southeast and northeast-southwest faults which displaced both the Kalahari Group and the Karoo Supergroup (Andreoli et al., 1996) (Figure 13f). Contemporary neotectonics show that southern Africa is presently in a state of horizontal extension and, therefore, prone to normal faulting (Westgate et al., 2021). The final stages of the model involved erosion of the land surface to the present day.

Conclusion

To constrain the subsurface geology of the KMF, the depth of the Hotazel Formation, where the Mn ore is hosted, and the structures associated with upgrading the Mn ore, high-resolution 2D reflection surveys were conducted in the Severn area of the KMF. The contacts between the various lithologies of the (1) Ventersdorp and Transvaal supergroups, (2) Campbellrand and Schmidtsdrif subgroups and Asbestos Hills and Koegas subgroups, (3) Ghaap and Postmasburg groups, (4) Makganyene and Ongeluk formations, (5) Ongeluk and Hotazel formations, (6) Hotazel and Mooidraai formations, (7) Transvaal and Keis supergroups (the pre-Gamagara unconformity), (8) Keis and Karoo supergroups, and (9) Karoo

Downloaded from http://pubs.geoscienceworld.org/gssa/sajg/article-pdf/128/1/53/7237934/53_0003_jogee_et_al.pdf?casa_token=YSLKsPTCYswAAAAA:_v2NFIsneibQLQBcqZKIsf2DmEiRjMF4t6wGBtd96Jv4JPsio5HLMrbL
by University of the Witwatersrand user

Supergroup and Kalahari Group, have been constrained. The pre-Gamagara unconformity was mapped at a depth of approximately 0.7 km and is significant as the unconformity allowed fluids to percolate downwards causing supergene enrichment of the Mn ore during the Palaeoproterozoic. Several structures are present on seismic section P1 which strike north-south, northeast-southwest and northwest-southeast. The north-south striking structures are interpreted as dolerite dykes. Imaging the dolerite dykes is important for mine planning as the dykes potentially lowers the grade of the ore and can also cause major disruptions in the stratigraphy. The northeast-southwest and northwest-southeast striking structures are interpreted as reactivated normal faults and shallow dipping listric thrust faults that "stacked" or "duplicated" the lithologies. The reactivated normal faults served as conduits for mineral rich fluids which caused major upgrades of the Mn ore. The mapped reactivated structures can be used to target areas with similar orientated structures to locate the high-grade Mn ore associated with these structures. The Kalahari unconformity, where in direct contact with the Hotazel Formation, could be another exploration horizon for moderately upgraded Mn ore. Results from this work demonstrate that high-resolution seismics is a powerful tool to image the subsurface geology of the KMF. Reflection seismics is effective in mapping the subsurface geology and structures within the KMF to target areas for exploration and for mine plan designing ensuring maximum production.

Declaration of competing interest

The authors declare that they have no known competing interests that could have appeared to influence the work.

Data availability

The data were acquired by the Wits Seismic Research team and are available upon request.

Acknowledgements

We would like to acknowledge African Exploration Mining and Finance Corporation (AEMFC) for funding this research project. The authors would like to thank the team from the Wits Seismic Research Centre of the School of Geosciences at the University of the Witwatersrand (South Africa) for assisting with data collection. The Department of Science and Innovation-National Research Foundation Centre of Excellence in Mineral and Energy Resource Analysis (DSI-NRF CIMERA) is thanked for financial support. We would also like to thank SLB for the support with Petrel software licences. We are furthermore grateful for Petrosys for supporting the Centre with the GLOBEClaritas software licences that were used for seismic data processing. We thank anonymous reviewers and SAJG Editorial team for their constructive comments and editorial support that improved the quality of this paper.

References

Altermann, W. and Schopf, J.W., 1995. Microfossils from the Neoarchaean Campbell Group, Griqualand West Sequence of the Transvaal Supergroup, and their palaeoenvironmental and evolutionary implications. Precambrian Research, 75, 65-90.

Andreoli, M.A.G., Van Bever Donker, J., Brandt, D. and Andersen., N.J.B., 1996. Neotectonics of southern Africa- a review. Africa Geoscience Review, 3, 1-16.

Angerer, T., Thorne, W., Hagemann, S.G., Tribus, M., Evans, N.J. and Savard, D., 2022. Iron oxide chemistry supports a multistage hydrothermal genesis of BIF-hosted hematite ore in the Mt. Tom Price and Mt. Whaleback deposits. Ore Geology Reviews, 144, 104840.

Bangert, W., Stollhofen, H., Lorenz, V. and Armstrong, R., 1999. The geochronology and significance of ash-fall tuffs in the glaciogenic Carboniferous-Permian Dwyka Group of Namibia and South Africa. Journal of African Earth Sciences, 29, 33-49.

Bau, M., Romer, R.L., Lüders, V. and Beukes, N.J., 1999. Pb, O, and C isotopes in silicified Mooidraai dolomite (Transvaal Supergroup, South Africa): implications for the composition of Palaeoproterozoic seawater and 'dating' the increase of oxygen in the Precambrian atmosphere. Earth and Planetary Science Letters, 174, 43-57.

Beukes, N.J. and Gutzmer, J., 2008. Origin and palaeoenvironmental significance of major iron formations at the Archaean-Palaeoproterozoic boundary. Reviews in Economic Geology, 15, 5-47.

Beukes, N.J., 1980. Lithofacies and Stratigraphy of the Kuruman and Griquatown iron formations, northern Cape Province, South Africa.South African Journal of Geology, 83, 69-86.

Beukes, N.J., 1987. Facies relations, depositional environments and diagenesis in a major early Proterozoic stromatolitic carbonate platform to basinal sequence, Campbellrand Subgroup, Transvaal Supergroup, Southern Africa. Sedimentary Geology, 54, 1-46.

Beukes, N.J., Swindell, E.P. and Wabo, H., 2016. Manganese deposits of Africa. Episodes Journal of International Geoscience, 39, 285-317.

Beukes, NJ and Smit, C.A., 1987. New evidence for thrust faulting in Griqualand West, South Africa: implications for stratigraphy and the age of red beds. South African Journal of Geology, 90, 378-394.

Botha, G.A., 2021. Cenozoic stratigraphy of South Africa: current challenges and future possibilities. South African Journal of Geology, 124,817-842.

Cairncross, B. and Beukes, N., 2013. The Kalahari Manganese Field: the adventure continues. Struik Nature. Cape Town. South Africa.

Cairncross, B., Beukes, N.J. and Gutzmer, J., 1997. The Manganese Adventure: The South African Manganese Fields. Associated Ore and Metal Corporation Limited. South Africa.

Chopra, S. and Marfurt, K.J., 2005. Seismic attributes – A historical perspective. Geophysics, 70, 3-28.

Chopra, S. and Marfurt, K.J., 2008. Emerging and future trends in seismic attributes. The Leading Edge, 27, 298-318.

Coetzee, L.L., Gutzmer, J., Smith, A.J.B. and Beukes, N.J., 2024. Mineralogy and mineral paragenesis of the Palaeoproterozoic manganese ores of the Avontuur deposit of the Kalahari Manganese Field, South Africa. South African Journal of Geology, 127, 31-54.

Cornell, D., Zack, T., Anderson, F., Corfu., Feri., D. and Schijndel, V., 2016. The U-Pb zircon geochronology of the Palaeoproterozoic Hartley Formation porphyry by six methods, with age uncertainty approaching 1 Ma. South African Journal of Geology, 119, 473-494.

Cox, D.R., Newton, A.M. and Huuse, M., 2020. An introduction to seismic reflection data: Acquisition, processing and interpretation. In: N. Scarselli, J. Adam and D. Chiarella (Editors), Regional geology and tectonics: Principles of Geologic Analysis, 2nd edition, volume 1, Elsevier, 571-603.

Crow, C. and Condie, K.C., 1988. Geochemistry and origin of late Archaean volcanics from the Ventersdorp Supergroup, South Africa. Precambrian Research, 42, 19-37.

Czaja, A.D., Beukes, N.J. and Osterhout, J.T., 2016. Sulfur-oxidizing bacteria prior to the great oxidation event from the 2.52 Ga Gamohaan formation of South Africa. Geology, 44, 983-986.

Dalstra, H.J. and Rosière, C.A., 2008. Structural controls on high-grade iron ores hosted by banded iron formation: a global perspective. Reviews in Economic Geology, Vol. 15, Society of Economic Geologists, Littleton, 73-106.

Downloaded from http://pubs.geoscienceworld.org/gssa/sajg/article-pdf/128/1/53/7237934/53_0003_jogee_et_al.pdf?casa_token=YSLKsPTCYswAAAAA:_v2NFIsneibQLQBcqZKIsf2DmEiRjMF4t6wGBtd96Jv4JPsio5HLMrbL
by University of the Witwatersrand user

De Kock, M.O., Monareng, B.F., Blignaut, L., Smith, A.J.B. and Beukes, N.J., 2020. Geochemistry of Palaeoproterozoic saprolite developed in diabase intruding the Hotazel Formation in the Avontuur deposit of the Kalahari Manganese Field, South Africa. South African Journal of Geology 2020, 123, 1-18.

Eriksson, P.G., Altermann, W. and Hartzer, F.J., 2006. Chapter 10: The Transvaal Supergroup and its precursors, In: M.R. Johnson, C.R. Anhaeusser and R.J. Thomas (Editors), The geology of South Africa. South African Council for Geosciences and the Geological Society of South Africa, 237-260.

Evans, D.A., Beukes, N.J. and Kirschvink, J.L., 1997. Low-latitude glaciation in the Palaeoproterozoic era. Nature, 386, 262-266.

Gumsley, A.P., Chamberlain, K.R., Bleeker, W., Söderlund, U., De Kock, M.O., Larsson, E.R. and Bekker, A., 2017. Timing and tempo of the Great Oxidation Event. Proceedings of the National Academy of Sciences, 114, 1811-1816.

Gutzmer, J. and Beukes, N.J., 1995. Fault-controlled metasomatic alteration of early Proterozoic sedimentary manganese ores in the Kalahari manganese field, South Africa. Economic Geology, 90, 823-844.

Gutzmer, J. and Beukes, N.J., 1996a. Mineral paragenesis of the Kalahari Manganese Field, South Africa. Ore Geology Reviews 11. 405-428.

Gutzmer, J. and Beukes, N.J., 1996b. Karst-hosted fresh-water Palaeoproterozoic manganese deposits, Postmasburg, South Africa. Economic Geology, 91, 1435-1454.

Gutzmer, J. and Beukes, N.J., 1998. The manganese formation of the Neoproterozoic Penganga Group, India; revision of an enigma. Economic Geology, 93,1091-1102.

Gutzmer, J., Du Plooy, A.P. and Beukes, N.J., 2012. Timing of supergene enrichment of low-grade sedimentary manganese ores in the Kalahari Manganese Field, South Africa. Ore Geology Reviews, 47, 136-153.

Havenga, M., 2014. Delineating possible Mn and iron ore target areas for further surveying on selected farms in the Kuruman district. African Exploration Mining and Finance Corporation SOC Ltd (AEMFC).

Hongjun, Z., Weibo, Z., Xiufa, C., Xuezhou, H.E., Chao, Z., Chao, C., Yongshan, Y.U. and Yulin, Z., 2022. Genetic types, geological characteristics and genetic mechanism of manganese deposits in Africa. Geology in China, 49, 81-102.

Kendall, B., van Acken, D. and Creaser, R.A., 2013. Depositional age of the early palaeoproterozoic klipputs member, nelani formation (Ghaap Group, Transvaal Supergroup, South Africa) and implications for low-level Re-Os geochronology and palaeoproterozoic global correlations. Precambrian Research, 237, 1-12.

Kirschvink, J.L., Gaidos, E.J., Bertani, L.E., Beukes, N.J., Gutzmer, J., Maepa, L.N. and Steinberger, R.E., 2000. Palaeoproterozoic snowball Earth: Extreme climatic and geochemical global change and its biological consequences. Proceedings of the National Academy of Sciences, 97, 1400-1405.

Klein, C., 2005. Some Precambrian banded iron-formations (BIFs) from around the world: Their age, geologic setting, mineralogy, metamorphism, geochemistry, and origins. American Mineralogist, 90, 1473-1499.

Kunzmann, M., Gutzmer, J., Beukes, N.J. and Halverson, G.P., 2014. Depositional environment and lithostratigraphy of the Palaeoproterozoic Mooidraai Formation, Kalahari manganese field, South Africa. South African Journal of Geology, 117, 173-192.

Le Heron, D.P., Busfield, M.E., Smith, A.J.B. and Wimmer, S., 2022. A grounding zone wedge origin for the Palaeoproterozoic Makganyene Formation of South Africa. Frontiers in Earth Science, 10, 905602.

Malehmir, A. and Bellefleur, G., 2010. Reflection seismic imaging and physical properties of base-metal and associated iron deposits in the Bathurst Mining Camp, New Brunswick, Canada. Ore Geology Reviews, 38, 319-333.

Maries, G., Malehmir, A., Bäckström, E., Schön, M. and Marsden, P., 2017. Downhole physical property logging for iron-oxide exploration, rock quality, and mining: An example from central Sweden. Ore Geology Reviews, 90, 1-13.

Markovic, M., Maries, G., Malehmir, A., von Ketelhodt, J., Bäckström, E., Schön, M. and Marsden, P., 2020. Deep reflection seismic imaging of iron-oxide deposits in the Ludvika mining area of central Sweden. Geophysical Prospecting, 68, 7-23.

Mhlanga, X.R., Tsikos, H., Lee, B., Rouxel, O.J., Boyce, A.C., Harris, C. and Lyons, T.W., 2023. The Palaeoproterozoic Hotazel BIF-Mn Formation as an archive of Earth's earliest oxygenation. Earth-Science Reviews, 240, 104389.

Mitchum Jr, R.M., Vail, P.R. and Thompson III, S., 1977. Seismic stratigraphy and global changes of sea level: Part 2. The depositional sequence as a basic unit for stratigraphic analysis: Section 2. In: Pyton, C.E. (Editor). Application of seismic reflection configuration to stratigraphic interpretation, American Association of Petroleum Geologists, 53-62.

Mudau, M.T., 2020. Manganese genesis, analysis and future demand: A case study from the United Manganese of Kalahari (UMK), Hotazel, South Africa, PhD thesis, University of the Witwatersrand.

Nel, C.J.J., Beukes, N.J. and de Villiers, J.P.R., 1986. The Mamatwan manganese mine of the Kalahari manganese field. In: C.R. Anhaeusser and S. Maske (Editors), Mineral Deposits of Southern Africa. Johannesburg, Geological Society of South Africa, 1, 963-978.

Papadopoulos, V., 2023. Dating, isotope fingerprinting and metallogenic role of alkali metasomatism in Fe and Mn-rich rocks of the Northern Cape, South Africa, PhD thesis, University of Glasgow.

Poli, T., 2011. Gravenhage Manganese Project Definitive Feasibility Study Completed., ASX Release.

Randen, T., Pedersen, S.I. and Sønneland, L., 2001. Automatic extraction of fault surfaces from three-dimensional seismic data. In Society of Exploration Geophysicists International Exposition and Annual Meeting, Society of Exploration Geophysicists, Society of Exploration Geophysicists-2001.

Rasmussen, B., Muhling, J.R., Zi, J.W., Tsikos, H. and Fischer, W.W., 2020. A 1.25 Ga depositional age for the "Palaeoproterozoic" Mapedi red beds, Kalahari manganese field, South Africa: new constraints on the timing of oxidative weathering and hematite mineralisation. Geology, 48, 44-48.

Richards, P.K., 2021. Petrographical, Mineralogical and Geochemical Characterisation of the Leinster Deposit, Kalahari Manganese Field, South Africa. Unpublished M.Sc. thesis. University of Johannesburg, 155.

Schnebele, E.K., 2023. U.S. Geological Survey, Mineral Commodity Summaries, January 2023. Manganese, 2.

Schröder, S., Bedorf, D., Beukes, N.J. and Gutzmer, J., 2011. From BIF to red beds: Sedimentology and sequence stratigraphy of the Palaeoproterozoic Koegas Subgroup (South Africa). Sedimentary Geology, 236, 25-44.

Smith, A.J.B. and Beukes, N.J., 2016. Palaeoproterozoic banded iron formation-hosted high-grade hematite iron ore deposits of the Transvaal Supergroup, South Africa. Episodes Journal of International Geoscience, 39, 269-284.

Smith, A.J.B. and Beukes, N.J., 2023. The palaeoenvironmental implications of pre-Great Oxidation Event manganese deposition in the Mesoarchaean Ijzermijn Iron Formation Bed, Mozaan Group, Pongola Supergroup, South Africa. Precambrian Research, 384, 106922.

Smith, A.J.B., Beukes, N.J., Cochrane, J.M. and Gutzmer, J., 2023. Manganese carbonate-bearing mudstone of the Witwatersrand-Mozaan succession in southern Africa as evidence for bacterial manganese respiration and availability of free molecular oxygen in Mesoarchaean oceans. South African Journal of Geology 2023, 126, 29-48.

Smith, A.J.B., Gutzmer, J., Beukes, N.J. and Chisonga, B.C., 2019. Iron ore of the Hotazel Formation, Northern Cape Province, South Africa. In: Iron Ore 2019, Perth, WA, 22-24 July 2019, Australian Institute of Mining and Metallurgy Publication Series No3/2019, 414-433.

Tsikos, H. and Moore, J.M., 1997. Petrography and geochemistry of the Palaeoproterozoic Hotazel Iron-Formation, Kalahari manganese field, South Africa; implications for Precambrian manganese metallogenesis. Economic Geology, 92, 87-97.

Tsikos, H., Beukes, N.J., Moore, J.M. and Harris, C., 2003. Deposition, diagenesis, and secondary enrichment of metals in the Palaeoproterozic Hotazel iron-formation, Kalahari Manganese Field, South Africa. Economic Geology, 98, 1449-1462.

Tsikos, H., Matthews, A., Erel, Y. and Moore, J.M., 2010. Iron isotopes constrain biogeochemical redox cycling of iron and manganese in a Palaeoproterozoic stratified basin. Earth and Planetary Science Letters, 298, 125-134.

Tsikos, H., Moore, J.M. and Harris, C., 2001. Geochemistry of the Palaeoproterozoic Mooidraai formation: Fe-rich limestone as end member of iron formation deposition, Kalahari manganese field, Transvaal

Downloaded from http://pubs.geoscienceworld.org/gssa/sajg/article-pdf/128/1/53/7237934/53_0003_jogee_et_al.pdf?casa_token=YSLKsPTCYswAAAAA:_v2NFIsneibQLQBcqZKIsf2DmEiRjMF4t6wGBtd96Jv4JPsio5HLMrbL
by University of the Witwatersrand user

Supergroup, South Africa. Journal of African Earth Sciences, 32, 19-27.

Vafeas, N.A., 2016. Petrography and Geochemistry of the Hotazel Formation on Mukulu 265, Kalahari Manganese Field, Northern Cape Province. MSc thesis, University of Johannesburg.

Vafeas, N.A., Blignaut, L.C., Viljoen, K.S. and Meffre, S., 2018. New evidence for the early onset of supergene alteration along the Kalahari unconformity. South African Journal of Geology, 121, 157-170.

Van Niekerk, H.S. and Beukes, N.J., 2019. Revised definition/outline of the Kheis Terrane along the western margin of the Kaapvaal Craton and lithostratigraphy of the newly proposed Keis Supergroup. South African Journal of Geology, 122, 187-220.

Van Niekerk, H.S., 2006, The origin of the Kheis Terrane and its relationship with the Archaean Kaapvaal Craton and Greenvillian Namaqua Province in Southern Africa, unpublished PhD thesis, University of Johannesburg, 402.

Walraven, F. and Martini, J., 1995. Zircon Pb-evaporation age determinations of the Oak Tree Formation, Chuniespoort Group, Transvaal Sequence: implications for Transvaal-Griqualand West basin correlations. South African Journal of Geology, 96, 58-67.

Westgate M., 2020. Reappraisal of legacy reflection seismic data using advanced processing techniques and seismic attributes, PhD thesis, University of the Witwatersrand, South Africa.

Westgate, M., Manzi, M.S., Malehmir, A., Gibson, R.L., Andreoli, M.A. and Bumby, A., 2021. A reappraisal of legacy reflection seismic data from the western margin of the Kaapvaal craton, South Africa, with implications for Mesozoic-Cenozoic regional tectonics. Tectonophysics, 813, 228934.

Editorial handling: M.A. Elburg.

Downloaded from http://pubs.geoscienceworld.org/gssa/sajg/article-pdf/128/1/53/7237934/53_0003_jogee_et_al.pdf?casa_token=YSLKsPTCYswAAAAA:_v2NFIsneibQLQBcqZKIsf2DmEiRjMF4t6wGBtd96Jv4JPsio5HLMrbL
by University of the Witwatersrand user